A thesisfor the degree ofDoctor of Philosophy

Heave motion response of a floating offshore windturbine with damping plate

Hyeok-Jun Koh

Multidisciplinary Graduate School for Wind Energy

GRADUATE SCHOOL

JEJU NATIONAL UNIVERSITY

2014. 8.

Heave motion response of a floating offshore wind turbine with damping plate

Hyeok-Jun Koh

(Supervised by professor Il-Hyoung Cho)

A thesis submitted in partial fulfillment of the requirementfor the degree of Doctor of Philosophy

2014. 6.

This thesis has been examined and approved by

Thesis director, Jong-ChulHur, Professor,Dept. of Mechanical Engineering

---

Yoon HyeokBae,AssistantProfessor,Dept. of Ocean System Engineering

---

Il-Hyoung Cho,Professor,Dept. of Ocean System Engineering

Dong-GukPaeng, Associate Professor,Dept. of Ocean System Engineering

---

Nam-Ho Kyong, Principal Researcher, Korea Institute of Energy Research

---

Date

Multidisciplinary Graduate School for Wind Energy
GRADUATE SCHOOL
JEJU NATIONAL UNIVERSITY

CONTENTS

CONTENTS ..... **iii**

LIST OF FIGURES ..... **vi**

LIST OF TABLES ..... **xii**

ABSTRACT ..... **xiii**

Chapter 1 INTRODUCTION **1**

1.1 Background and literature review 1

1.2Objectives 8

1.3Layout of thesis 10

Chapter 2 ANALYTIC SOLUTION **12**

2.1 A circular cylinder with a damping plate 12

2.1.1 Diffraction problem 14

2.1.2 Radiation problem 20

2.2 A circular cylinder with a rigid and a porous damping plates 23

2.2.1 Diffraction problem 25

2.2.2 Radiation problem 31

2.3 Equation of heave motion 33

2.3.1 Frequency domain analysis 33

2.3.2 Time domain analysis 34

Chapter 3 DISCRIPTION OF EXPERIMENT **39**

3.1 Free decay test.....39

3.1.1 Introduction.....39

3.1.2Experimental set-up.....41

3.2 Model test in regular waves.....48

3.2.1 Introduction.....48

3.2.2Experimental set-up.....48

3.3 Model test in irregular waves.....51

3.3.1 Introduction.....51

3.3.2Experimental set-up.....51

Chapter 4 RESULTS AND DISCUSSION.....58

4.1 Introduction.....58

4.2 Comparisons.....59

4.3Free decay test.....65

4.4Heave motion response in regular waves.....68

4.5 Heave motion response in irregular waves.....74

Chapter 5 APPLICATION TO A FLOATING OFFSHORE WIND TURBINE USING FAST CODE.....79

5.1 Introduction.....79

5.2 Model.....81

5.2.1Wind turbine.....81

5.2.2 Platform 82

5.2.3 Environmental conditions 86

5.3 Results 89

Chapter 6 CONCLUSIONS AND FUTURE WORK 100

REFERENCES 103

ACKNOWLEDGEMENT (IN KOREAN) 110

LIST OF FIGURES

Fig. 1.1. Types of floating support platform. (a) Semi-submersible, (b) Spar, (c) TLP 3

Fig. 1.2. Conceptual sketch of a cylinder with a damping plate. (a) a single rigid damping plate, (b) dual (rigid and porous) damping plates. 7

Fig. 2.1. Definition sketch of a circular cylinder with a damping plate. 14

Fig. 2.2. Definition sketch of the circular cylinder with dual (rigid and porous) damping plates. 24

Fig. 3.1. Time history of heave motion by a heave free decay test. 40

Fig. 3.2. The position of the cylinder with dual rigid damping plates for the heave free decay test in steel water. (a) equivalent position, (b) initial position with the 560g weight. 41

Fig. 3.3. The experimental model. (a) 3D drawing, (b) fabricated shape. 42

Fig. 3.4. Schematic sketch of the heave free decay test setup. (a) plane view, (b) elevation view. 44

Fig. 3.5. Wave generating system of the JNU wave tank. (a) piston-type wave maker, (b) inclined porous plate wave absorber. 44

Fig. 3.6. Vision tracking system. (a) targets of the model, (b) camera. 45

Fig. 3.7. Mooring configuration of the experimental model. (a) plane view, (b) elevation view. 45

Fig. 3.8. The experimental model installed in the JNU wave tank. 46

Fig. 3.9. Schematic drawings for the parameter selection of the damping plate attached on the experimental model. (a) position and diameter ratio, (b) porosity of the upper-plate.....46

Fig. 3.10. Schematic sketch of the regular wave test setup. (a) plane view, (b) elevation view. 49

Fig. 3.11. Capacitance-type wave gauge installed on the JNU wave tank. 50

Fig. 3.12. The experimental model for the irregular wave test. (a) 3D drawing, (b) fabricated model. 52

Fig. 3.13. Schematic sketch of the irregular wave test setup. 54

Fig. 3.14. Wave generating system of the SNU wave tank. (a) plunger-type wave maker, (b) beach-type wave absorber. 55

Fig. 3.15. Mooring configuration of the experimental model for the irregular wave test. 55

Fig. 3.16. The experimental model installed in the SNU wave tank. 56

Fig. 3.17. Measurement system. (a) accelerometer (AS-1GB), (b) surbo-type wave gauge. .56

Fig. 4.1. The S&N model. (a) definition sketch, (b) fabricated model. 59

Fig. 4.2. Comparison of heave RAO of classic spar with a single damping plate from MEEM with experimental and numerical results (Sudhakar and Nallayarasu, 2013). 61

Fig. 4.3. Comparison of heave RAO of classic spar with dual rigid damping plates from MEEM with experimental and numerical results (Sudhakar and Nallayarasu, 2013). 61

Fig. 4.4. Heave added mass due to an oscillating classic spar with dual damping plates according to the porosity of the upper-damping plate. 63

Fig. 4.5. Heave damping coefficient due to an oscillating classic spar with dual damping plates according to the porosity of the upper-damping plate. 63

Fig. 4.6. Heave wave exciting force on the classic spar with dual damping plates according to the porosity of the upper-damping plate. 64

Fig. 4.7. Non-dimensional damping coefficients from the free decay test as function of porosity and depth ratio for diameter ratio ($a / b = 1.6$). 66

Fig. 4.8. Non-dimensional damping coefficients from the free decay test as function of diameter and depth ratio for porosity ($P = 0.1$). 67

Fig. 4.9. Comparison of heave RAO among analytic (MEEM), numerical (AQWA), and experimental (Exp) results in case of cylinder only ($a / b = 1.6$). 69

Fig. 4.10. Comparison of heave RAO among analytic (MEEM), numerical (AQWA), and experimental (Exp) results in case of cylinder with a single plate attached at the bottom of the circular cylinder ($a / b = 1.6$). 69

Fig. 4.11. Comparison of heave RAO between analytic (MEEM) and experimental (Exp) results in case of cylinder with dual rigid damping plates for different depth ratios

of the upper-damping plate (a / b =1.6).....70

Fig. 4.12. Comparison of heave RAO between analytic (MEEM) and experimental (Exp) results in case of cylinder with dual damping plates for different depth ratio of the porous (P =0.1) upper-damping plate (a / b =1.6).....71

Fig. 4.13. Heave RAO of the circular cylinder with dual damping plates for different porosities of the upper-damping plate at position 1 (a / b =1.6). 72

Fig. 4.14. Heave RAO of the circular cylinder with dual damping plates for different porosities of the upper-damping plate at position 2 (a / b =1.6). 73

Fig. 4.15. Heave RAO of the circular cylinder with dual damping plates for different porosities of the upper-damping plate at position 3 (a / b =1.6). 73

Fig. 4.16. Heave motion time history of the circular cylinder without damping plate. (a) experiment, (b) MEEM. (case104: ω_p =3.0 and H_s =0.102).....75

Fig. 4.17. Heave motion time history of the circular cylinder with damping plate. (a) experiment, (b) MEEM. (case203: ω_p =3.0 and H_s =0.102, a / b =1.6).....76

Fig. 4.18. Comparison of wave and heave motion spectrum between analytic and experimental results for the circular cylinder without the damping plate.....77

Fig. 4.19. Comparison of wave and heave motion spectrum between analytic and experimental results for the circular cylinder with a rigid damping plate.....78

Fig. 5.1. Interfacing modules to achieve aero-hydro-servo-elastic simulation (Jonkman, 2007).....80

Fig. 5.2. Comparison of heave added mass due to an oscillating spar type floating platform of the FOWT between analytical (MEEM) and numerical (AQWA) results. 84

Fig. 5.3. Comparison of heave radiation damping due to an oscillating spar type floating platform of the FOWT between analytical (MEEM) and numerical (AQWA) results. 84

Fig. 5.4. Comparison of heave wave exciting force on the spar type floating platform of the FOWT between analytical (MEEM) and numerical (AQWA) results. 85

Fig. 5.5. Heave RAO for the spar type FOWT with a single and dual ($P = 0.1$) damping plates and without a damping plate. 85

Fig. 5.6. JONSWAP wave spectrum ($\gamma = 3.3$) for each sea state. 87

Fig. 5.7. Wind speed time history ($V_{mean} = 11.4 \frac{m}{s}$, $Iref = 1$). 87

Fig. 5.8. Wave elevation time history ($H_s = 7.50 \frac{m}{s}$, $Tp = 15.0\,sec$). 88

Fig. 5.9. Heave motion time history of the FOWT for sea state 6 (H_s=5.0 m, T_p=12.4 sec). (a) without a damping plate, (b) with a single rigid damping plate (a/b=1.6), (c) with dual (rigid + porous) damping plates (a/b=1.6, d_0/d=0.54, P=0.1)...90

Fig. 5.10. Heave motion time history of the FOWT for sea state 7 (H_s=7.5 m, T_p=15.0 sec). (a) without a damping plate, (b) with a single rigid damping plate (a/b=1.6), (c) with dual (rigid + porous) damping plates (a/b=1.6, d_0/d=0.54, P=0.1)...91

Fig. 5.11. Heave motion spectrum of the spar type FOWT with a single and dual (d_0/d=0.54, P=0.1) damping plates and without a damping plate (a/b=1.6)

for sea state 6 (H_s =5.0 m, T_p =12.4 sec). 92

Fig. 5.12. Heave motion spectrum of the spar type FOWT with a single and dual (d_0 / d =0.54, P =0.1) damping plates (a / b =1.6) and without a damping plate for sea state 7 (H_s =7.5 m, T_p =15.0 sec). 93

Fig. 5.13. The tower base axial force time history of the FOWT for sea state 7 (H_s =7.5 m, T_p =15.0 sec). (a) without a damping plate, (b) with a single rigid damping plate (a / b =1.6), (c) with dual (rigid + porous) damping plates (a / b =1.6, d_0 / d =0.54, P =0.1).....95

Fig. 5.14. The yaw bearing axial force time history of the FOWT for sea state 7 (H_s =7.5 m, T_p =15.0 sec). (a) without a damping plate, (b) with a single rigid damping plate (a / b =1.6), (c) with dual (rigid + porous) damping plates (a / b =1.6, d_0 / d =0.54, P =0.1).....96

Fig. 5.15. The blade root axial force time history of the FOWT for sea state 7 (H_s =7.5 m, T_p =15.0 sec) in parked condition. (a) without a damping plate, (b) with a single rigid damping plate (a / b =1.6), (c) with dual (rigid + porous) damping plates (a / b =1.6, d_0 / d =0.54, P =0.1).....97

Fig. 5.16. The generated power time history of the FOWT for sea state 7 (H_s =7.5 m, T_p =15.0 sec). (a) without a damping plate, (b) with a single rigid damping plate (a / b =1.6), (c) with dual (rigid + porous) damping plates (a / b =1.6, d_0 / d =0.54, P =0.1).....99

LIST OF TABLES

Table 3.1. The specification of the experimental model.....42

Table 3.2. Experimental parameters in the free decay test. 47

Table 3.3. The regular wave conditions 50

Table 3.4. The specification of the experimental model for model test in irregular waves.....53

Table 3.5. The irregular wave condition.....57

Table 4.1. The specifications of the S&N model. 60

Table 5.1. Specifications of NREL 5MW wind turbine. 81

Table 5.2. Specifications of the spar type floating platform.....83

Table 5.3. Environmental conditions for each sea state. 86

Table 5.4. Statistical analysis results of the wave and the heave motion of the FOWT. 94

Table 5.5. Statistical analysis results of the axial forces on the FOWT.....98

ABSTRACT

A rigid damping plate attached to the bottom of a cylinder has a distinct advantage in reducing the motion response of a floating circular cylinder by increasing the added mass and the damping coefficient. The added mass plays an important role in determining the location of the resonant frequency, and also the radiation damping reduces the motion amplitude at resonance. Furthermore, the porous holes of the permeable damping plate induce flow separation and vortices agitation,causingthe increase of the viscous damping and energy loss. To obtain better heave characteristics, the present research proposes dual damping plates: a porous upper-damping plate attached to the side wall of the cylinder and a rigid lower-damping plate to the bottom.

Analytical and experimental studies are carried out to investigate the heave motion response of the cylinder according to the characteristics of the damping plate such as depth ratio, diameter ratio, and porosity. The analytical method by using Matched Eigenfunction Expansion Method (MEEM) has been developed for the heave motion analysis of the floating circular cylinder with the single rigid or dual (a rigid anda porous)damping plates in the context of linear potential theory and Darcy's law (the normal velocity of fluid passing through a thin porous disk is linearly proportional to the pressure difference across it).To apply the MEEM, the fluid domain is divided into three regions, and both the diffraction and the radiation potential in each region are expressed by the Fourier Bessel series. The unknown

coefficients in each region are determined by applying the continuity of the pressure and the normal velocity at the matching boundaries.With the assumption of an inviscid fluid in the potential theory, a heave viscous damping iscalculated by the non-dimensional damping coefficient obtained from aheave free decay test. In order to confirm the analytical solutions, experiments have been conducted in 2-D wave flume for the test in regular waves, and in large scaled wave flume for the test in irregular waves, with varying wave conditions.Theanalytical results are in good agreement with the experimental results in both regular and random waves, and the heave motion response of the cylinder is decreased drastically in the heave resonance region by the proposed dual damping plates.

In the application study of the damping plate to theFloating Offshore Wind Turbine (FOWT), the NREL offshore 5MW baseline wind turbine and spar type floating support structure are adopted to perform computational simulations using FAST code. The hydrodynamic input data of the floating support platform with a single rigid and dual(a rigid and a porous) damping platesfor HydroDyn,hydrodynamics module of FAST code, is calculated by the MEEM.The heave motion and the variation of the axial forces of the FOWT are considerably decreased ataround the heave resonantfrequency by the damping plate. It would be a great advantage to extend the fatigue life of the FOWT.In addition, it shifts the heave natural frequency to the lower frequency region due to the increase of the added mass. However, the decrease in the heave motion of the FOWT hardly affects the power generation.

Chapter 1

INTRODUCTION

1.1 Background and literature review

Major concerns of onshore wind turbine system such as noise, civil complaints, and spatial limitations bring the interest of offshore for an alternative installation site. Furthermore, an offshore environmental condition provides not only reducing the aerodynamic load by lower ground roughness, but also increasingthe capacity of wind turbine by avoiding such issues as transportation, installation, and visual effect.These are the reasons the offshore wind turbinehas come into the spotlight in the wind power industry. The offshore wind turbines installed to date are fixed type substructures by using monopile or conventional concrete gravity base in 20m depth of water, andtripod or jacket within40m depth of field.However, it affects fishing and sightseeing in coastal areas. Therefore, the development of deep water offshore wind farm bytheFloating Offshore Wind Turbine(FOWT) may be anticipated to be solved in order to overcome technical and economical weakness of the fixed type support structure.

The concept for large scale offshore floating wind turbines was introduced by Heronemus(1972).These systems could be deployed without any limitations of site conditions including high wind sites located further offshore in deep water. Numerous floating support platform configurations such as Spar, Tension Leg Platform (TLP), and

Semi-submersible used in the offshore oil and gas industries are possible for a FOWT (see Fig. 1.1).

For the design of theFOWT, the entire system composed of rotor, nacelle, tower, platform, and mooring system; subjected to wind, wave and hydrodynamic loads should be analyzed using integrated models (Nielson et al., 2006). Jonkman (2007) discussed dynamic response for theFOWT with a barge platform using an analytical model for Catenary mooring system.The specific properties of Hywind, the first full-scale spar type FOWT, provided by OC3 project have been used to analyze and investigate performance characteristics of the spar type FOWT by numerical (Nielsen et al., 2006; Skaare et al., 2007; Larsen and Hanson, 2007, Jonkman, 2009) and experimental (Shin, 2011; Myhr et al., 2011) methods.Waris and Ishihara (2012) developed a finite element model to investigate a dynamic response of floating offshore wind turbine system. Also, the effects of a single damping plate, applicability of linear and nonlinear models for dynamic response prediction of catenary and tension leg mooring system on floater response were discussed.

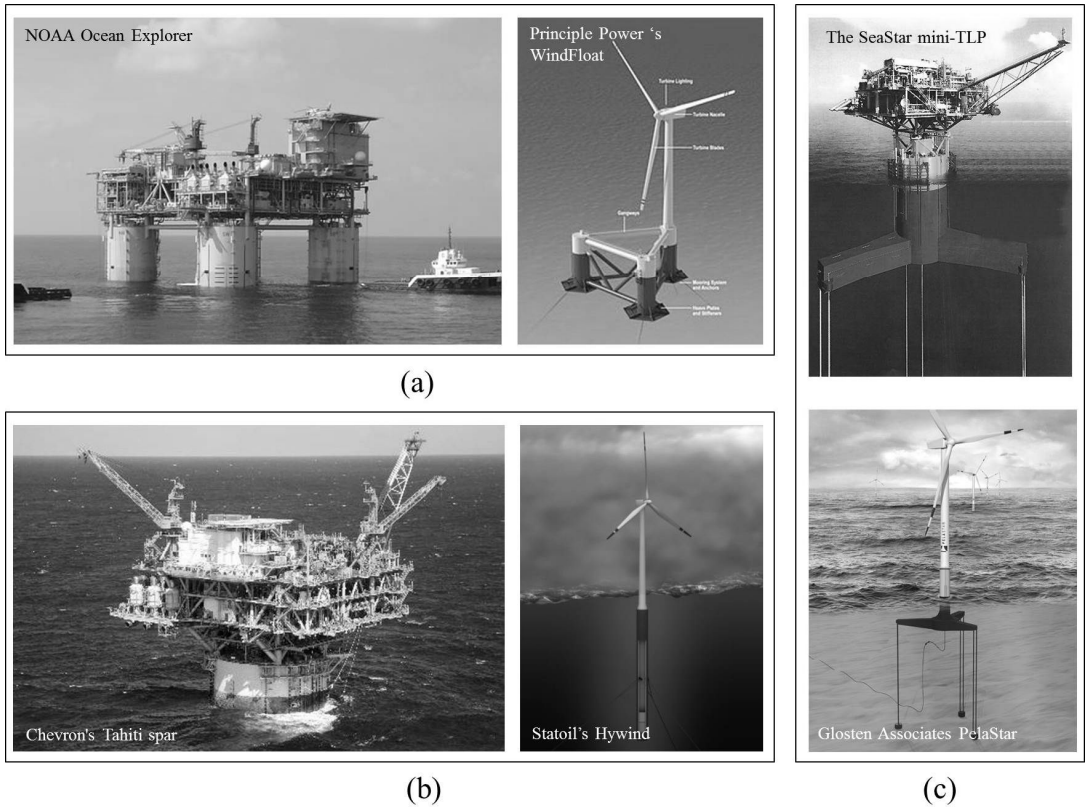

Fig.1.1. Types of floating support platform. (a) Semi-submersible, (b) Spar, (c) TLP

An analysis on hydrodynamic force by the movement of a floating structure has been carried out by many researchers. Havelock (1955) analyzed the added mass and damping coefficient of a sphere floating on the free surface using a multipole expansion method. Mei and Black (1969) solved the radiation problem and diffraction problem of a 2-D floating square structure. In order to reduce wave forces and motion of the floating structure, the majority of offshore platform structures have cylinder type substructures. Thus, the analysis of motion responses on a circular cylinder is one of the most important parts for the offshore

platform design. Bai (1977) presented numerical results for the added mass and damping of a semi–submerged two-dimensional heaving cylinder in the water of finite depth. The scattering problem of a cylinder was dealt with Garrett (1971) and the radiation problem was analyzed by Tung (1979) and McIver and Evans (1984). In addition, Kritis (1979) applied the hybrid method of Yeung (1975) to axisymmetric body and gave numerical results for a circular cylinder. Yeung (1981) gave the added mass and damping of a vertical cylinder in finite–depth waters.

An excessive heave motion is the result of a resonance which is generated when the natural frequency of the structure and the frequency of incident waves coincide. It is often to cause severe damage in mooring system. The basic concept of reducing the motion response of a floating structure is to increase the damping energy of the system by increasing the radiation and the viscous damping, or to move the natural frequency of the structure out of the frequency range of incident waves by increasing added mass.A damping plate installed at the bottom of the cylinder has a distinct advantage in reducing the motion responses of a floating circular cylinder by increasing the added mass and dampingas shown in Fig. 1.2 (a).Thiagarajan and Troesch (1998) observed the flow around the cylinder with a damping plate configuration using the particle image velocimetry(PIV) technique. Rho et al. (2002) carried out model tests to investigate the heave and pitch motion characteristics by the moon pool, strakes and a damping plate of a spar platform. Also they confirmed Mathieu-type instability which occurs when the pitch natural period is twice to the heave natural period.

Tao and Cai (2004) investigated vortex shedding pattern and hydrodynamic forces arising from the flow separation and vortex shedding around a damping plate of a circular cylinder by solving Navier-Stokes equation. Cho (2011) and Koh and Cho (2011) analyzed the hydrodynamic forces (added mass and the damping coefficient) acting on a cylinder with a damping plate using the Matched Eigenfunction Expansion Method (MEEM).

Tao et al. (2007) calculated viscous flow by a spar hull with two solid damping plates of variable spacings using a finite difference method. The results showed that a significant influence of the spacing of the plates on the hydrodynamic is revealed clearly when it is smaller than the critical value. At very small relative spacing, the configuration of the plates is found to produce lower damping and added mass than a cylinder with a single damping plate. It is caused that the vortex shedding process between the two plates is suppressed at very small relative spacing. Sudhakar and Nallayarasu (2013, 2014) investigated the influence of single and double damping plates on the hydrodynamic response of a spar in regular and irregular waves by the experimental study. A truss spar with several damping plates attached to a under the hull was proposed and investigated by numerical (Stansberg et al., 2001; Sadeghi et al., 2004) and experimental (Downie et al., 2000; .Magee et al., 2000) methods.

To obtain better heave motion characteristics, the dual–damping plate, which is composed of a porous plate attached to the side wall and a solid plate at the bottom of the cylinder is proposed (see Fig. 1.2). The porous damping plate can induce energy

dissipationby increasingviscous flow through holes. There have been many theoretical and experimental studies regarding the energy dissipation by porous plates. For example, the wave transmission of a thin vertical porous plate placed in deep water was investigated by Tuck(1975). He discussed the application of Darcy's law for flows across porous plates and suggested that in the case of sinusoidal oscillations the velocity across the material with fine pores can be related to the pressure drop by a complex-valued frequency dependent parameter, which accounts for both viscous and inertial effects. The same porosity model was also used by Chwang(1983), Chwang and Wu(1994), Yu(1995), Wang and Ren(1994). Molin and Nielsen(2004) investigated the hydrodynamic characteristics of a perforated disk below the free surface based on the potential theory. They applied a quadratic relationship between the pressure difference and normal velocity. The amplitude dependent hydrodynamic coefficients are in good agreement with experimental results.In the case of wave interaction with submerged porous plates, the Darcy's model was validated by Cho and Kim(2008) through small and large scale experiments.Tao and Dray(2008) investigated the hydrodynamic characteristics of oscillatory solid or porous disk using model–scale experiments.

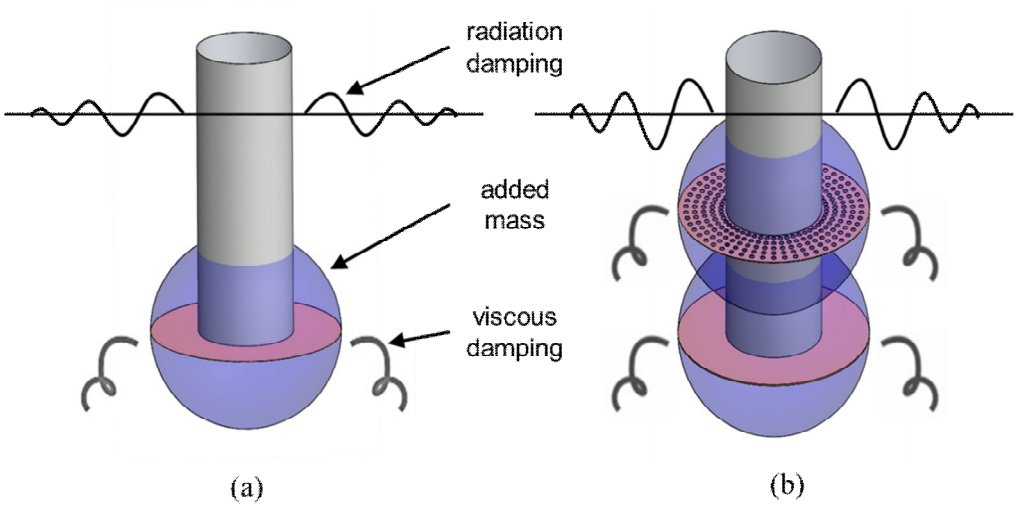

Fig.1.2. Conceptual sketch of a cylinder with a damping plate. (a) asingle rigid damping plate, (b) dual (rigid andporous) damping plates.

1.2Objectives

The previous researches about single and dual rigid damping plates have been carried out using numerical and experimental methods. In the experimental study, however, it requires too much time and high cost. Numerical calculations also require enormous computational time. Thus, the heave motion response of the cylinder is examined through an analytical method applied by the MEEM with regard to the variation of the characteristics of the single rigid and dualdamping plates. In the MEEM calculation, fluid domain is divided into three regions, and the velocity potentials in each region are expressed by the Fourier–Bessel series. The unknown coefficients in each region are determined by applying the continuity of pressure and normal velocity at the matching boundaries.

So far, there are no previous studies about the porous damping plate, attached to a cylinder,asa motion reduction device.In this research, the heave motion characteristics of circular cylinder with the porous damping plate are investigated based on the potential theory.The energy dissipation effect due to the porous damping plate is modeled by Darcy's law, which the normal velocity of fluid passing through a thin porous plate is linearly proportional to the pressure difference across it.The proportional coefficient, called porous parameter, was empirically determined from the experiments with the various types of porous plates by Cho and Kim (2008).

The viscous effect which is ignored by the assumption of the potential theory is considered experimentally for the analytical solution.The viscous damping is calculated from the non–dimensional damping coefficientobtained experimentally by a free decay test in still water. In addition, the verification is done for all analytical solution through model test in regular and irregular waves.

Finally, the NREL offshore 5MW baseline wind turbine model (Jonkman et al., 2009) and thespar type floating support platform, scaled up to 100 times the experimental model,with single and dual damping plates are considered as the application model.In order to predict the heave motion response of the FOWT, it is simulated by the FASTwind turbine dynamic simulation tool(Jonkman and Buhl, 2005) withhydrodynamic coefficient including added mass and radiation dampingwhich were generated by the MEEM.To take into account the viscosity of the damping plate, the viscous damping obtained by the free decay test in this research is added toHydroDyn, hydrodynamics module of FAST code.

1.3Layout of thesis

In the chapter, an introduction of the motivation and aims of this study are included. The literature reviews of research on the cylinder type floating body and motion reduction devices are also given.

Chapter 2 providesthe analytical formulationof matched eigenfunction expansion method for two cases, a cylinder with single damping plate and dual (rigid and porous) damping plates.

Chapter 3 describes the properties of the experimental models for the motion response tests in regular and irregular waves. Experimental setups of the heave free decay test and modeltest in regular and irregular waves are also given in this chapter.

In Chapter 4,the results of the heave motion of the circular cylinder with various damping platesfrom the series of experiments and analytical calculations are presented and discussed. In addition, the viscous damping coefficients measured fromthe heave free decay test is investigated by the comparisonswith thedepth ratio, the diameter ratio, and the porosity of the damping plate.

Chapter 5, the analytical results of the floating support structure with the damping plates are applied for the motion analysis of 5MW floating offshore wind turbine using FAST code.

Finally, concluding remarks and future studies related to the present work are given in Chapter 6.

Chapter 2

ANALYTIC SOLUTION

2.1 A circular cylinder with a damping plate

Using the MEEM, we solved the diffraction and radiation problem for a numerical model in which a circular damping plate with the diameter a was attached to the bottom of a cylinder with the radius b. For the analysis, the polar coordinate system (r,θ,z) is chosen with the origin on the undisturbed free surface and the z-axis pointing vertically upwards. The water depth is denoted by h, the distance between the bottom of the cylinder and seabed by $c=h-d$, and the draft of a cylinder by d (see Fig. 2.1). The monochromatic incident waves with an amplitude A and the frequency ω approaches to the cylinder. The water is assumed to be incompressible and inviscid, so that the fluid particle motion can be described by the velocity potential. Assuming the harmonic motion of the frequency ω, the velocity potential heave motion responsecan be written as $\Phi(r,\theta,z,t)=\mathrm{Re}\left\{\phi(r,\theta,z)e^{-i\omega t}\right\}$, $z=\mathrm{Re}\left\{z_a e^{-i\omega t}\right\}$. In the present research, only a heave motion is considered. Therefore, the total velocity potential can be expressed by the sum of the diffraction and radiation potentials as follows:

$$\phi(r,\theta,z)=\phi_D(r,\theta,z)-i\omega z_a\phi_R(r,z), \tag{2.1}$$

where z_a represents the amplitude of the forced heave oscillation. The diffraction potential

ϕ_D includes the incident wave potential ϕ_I and the scatteringpotential ϕ_S, i.e. $\phi_D = \phi_I + \phi_S$. The radiation potential is represented by ϕ_R. Since the body is axisymmetric, the radiation problem is a function of r and z.

The potential $\phi_{D,R}$ satisfies Laplace's equation (2.2) in the fluid and the following boundary conditions Eqs. (2.3–2.7).

$$\nabla^2 \phi_{D,R} = 0, \qquad \text{in the fluid domain} \tag{2.2}$$

$$\frac{\partial \phi_{D,R}}{\partial z} - K\phi_{D,R} = 0, \ \left(K = \omega^2 / g\right) \qquad \text{on } z = 0 \tag{2.3}$$

$$\frac{\partial \phi_{D,R}}{\partial z} = 0, \qquad \text{on } z = -h \tag{2.4}$$

$$\lim_{r\to\infty} r^{1/2}\left(\frac{\partial \phi_{D,R}}{\partial r} - ik_1\phi_{D,R}\right) = 0, \tag{2.5}$$

$$\frac{\partial \phi_{D,R}}{\partial r} = 0, \qquad \text{on } r = b, -d \le z \le 0 \tag{2.6}$$

$$\begin{cases} \dfrac{\partial \phi_D}{\partial z} = 0, \\ \dfrac{\partial \phi_R}{\partial z} = 1, \end{cases} \qquad \text{on } r < 0,\ z = -d \tag{2.7}$$

where g is the gravity accelerationand k_1 is the incident wave number.

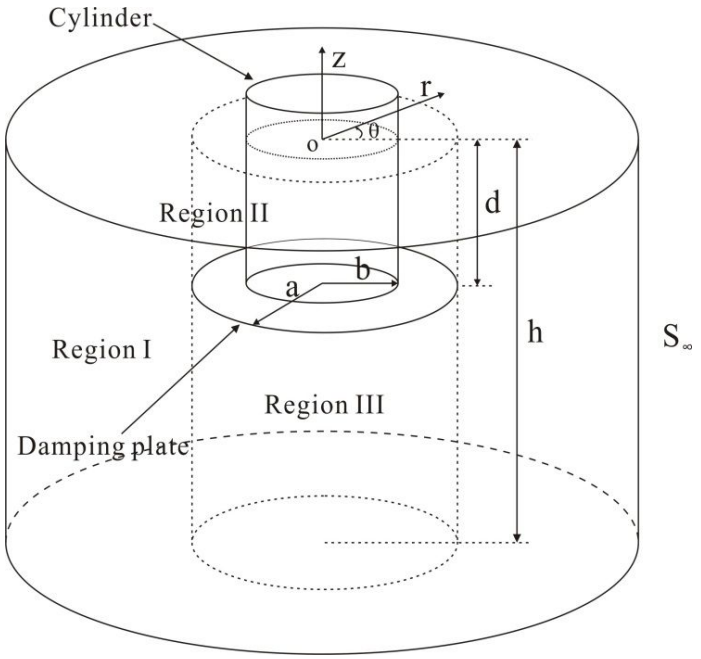

Fig.2.1.Definition sketch of a circular cylinder with a damping plate.

2.1.1 Diffraction problem

To apply the MEEM, the fluid domain is divided into three regions, as shown in Fig. 2.1, i.e. (I) the outer region $(r \geq a, -h \leq z \leq 0)$; (II) the upper inner region of the damping plate $(b \leq r \leq a, -d \leq z \leq 0)$; (III) the lower inner region of the damping plate $(0 \leq r \leq a, -h \leq z \leq -d)$. The diffraction potential is expressed by the separation of variables.

$$\phi_D(r,\theta,z) = -\frac{igA}{\omega}\sum_{l=0}^{\infty}\varphi_D^l(r,z)\cos l\theta. \tag{2.8}$$

In the outer region, the velocity potential satisfying Eqs.(2.2–2.5)can be written as:

$$\varphi_D^{l(1)}(r,z) = \beta_l J_l(k_1 r)\Gamma_0 f_{10}(z) + \sum_{n=0}^{\infty} A_{ln}^D \frac{K_l(k_{1n}r)}{K_l(k_{1n}a)} f_{1n}(z), \tag{2.9}$$

where $\Gamma_0 = N_{10}/\cosh k_1 h$ and β_l is defined by $\beta_0 = 1, \beta_l = 2(i)^l, l \geq 1$. J_l is the Bessel functions of the first kind and K_l is the modified Bessel functions of the second kind. The eigenvalues k_{1n} are the solution of the following dispersion equation.

$$k_{1n}\tan k_{1n}h = -\frac{\omega^2}{g}, \quad n = 0,1,2,\cdots \tag{2.10}$$

where $n=0$, $(k_{10} = -ik_1)$ term corresponds to an outgoing waves and $n \geq 1$ represents the evanescent waves. The eigenfunctions $f_{1n}(z)$ in Eq. (2.9) are given by

$$f_{1n}(z) = N_{1n}^{-1}\cos k_{1n}(z+h), \quad \text{with } N_{1n}^2 = \frac{1}{2}\left(1 + \frac{\sin 2k_{1n}h}{2k_{1n}h}\right) \tag{2.11}$$

and also satisfy the following orthogonality.

$$\frac{1}{h}\int_{-h}^{0} f_{1n}(z) f_{1m}(z)\,dz = \delta_{mn}, \tag{2.12}$$

where δ_{mn} is the Kronecker delta defined by $\delta_{mn} = 1$ if $m = n$, and $\delta_{mn} = 0$ if $m \neq n$.

In the region (II), the diffraction potential which satisfies body boundary conditions can

be written as follows:

$$\varphi_D^{I(2)}(r,z)=\sum_{n=0}^{\infty}B_{ln}^{D}\left(I_l(k_{2n}r)-\frac{I_l'(k_{2n}b)}{K_l'(k_{2n}b)}K_l(k_{2n}r)\right)f_{2n}(z), \quad (2.13)$$

where I_l is the modified Bessel function of the first kind. The prime appearing in the superscript denotes the derivative with respect to the argument. The eigenvalues $(k_{20}=-ik_2,\ k_{2n}, n=1,2,\cdots)$ in the region (II) are the roots of the dispersion relation $(k_{2n}\tan k_{2n}d=-\omega^2/g)$, and the normalized vertical eigenfunctions $f_{2n}(z)$ are defined as follows:

$$f_{2n}(z)=N_{2n}^{-1}\cos k_{2n}(z+d). \quad \text{with} \quad N_{2n}^2=\frac{1}{2}\left(1+\frac{\sin 2k_{2n}d}{2k_{2n}d}\right). \quad (2.14)$$

With the above definitions for $f_{1n}(z)$, it can be easily shown that the eigenfunctions satisfy the orthogonal relation.

$$\frac{1}{d}\int_{-d}^{0}f_{2n}(z)f_{2m}(z)dz=\delta_{mn}. \quad (2.15)$$

In the region (III), the diffraction potential takes the following form.

$$\varphi_D^{I(3)}(r,z)=\sum_{n=0}^{\infty}\varepsilon_n C_{ln}^{D}\frac{I_l(\lambda_n r)}{I_l(\lambda_n a)}\cos\lambda_n(z+h), \quad (2.16)$$

where ε_n is the Neumann symbol, defined by $\varepsilon_n=1$, if $n=0$, and $\varepsilon_n=2$, if $n\geq 1$, and

the eigenvalues in the region (III) is $\lambda_n = n\pi / c, \left(n = 0,1,2,\cdots\right)$.

The unknown coefficients A_{ln}^D, B_{ln}^D, C_{ln}^D $\left(n = 0,1,2,\cdots\right)$ in (2.9), (2.13), and (2.16) are determined by invoking the matching conditions. The continuity of velocity potential φ_D^l at $r = a$ requires

$$\beta_l J_l\left(k_1 a\right)\Gamma_0 f_{10}\left(z\right) + \sum_{n=0}^{\infty} A_{ln}^D f_{1n}\left(z\right) = \begin{cases} \sum_{n=0}^{\infty} B_{ln}^D s_{ln} f_{2n}\left(z\right), & -d \le z \le 0 \\ \sum_{n=0}^{\infty} \varepsilon_n C_{ln}^D \cos\lambda_n\left(z+h\right), & -h \le z \le -d \end{cases} \tag{2.17}$$

where

$$s_{ln} = I_l\left(k_{2n}a\right) - \frac{I_l'\left(k_{2n}b\right)}{K_l'\left(k_{2n}b\right)} K_l\left(k_{2n}a\right).$$

Multiplying both sides of Eq. (2.17) by the set of the functions $\cos\lambda_m\left(z+h\right)$, $m = 0,1,2,\cdots$ and integrate with respect to z over $\left[-h,-d\right]$, the following equation can be obtained.

$$C_{lm}^D = \sum_{n=0}^{\infty} A_{ln}^D G_{mn} + \beta_l J_l\left(k_1 a\right)\Gamma_0 G_{m0}, \; m = 0,1,2,\cdots \tag{2.18}$$

where

$$G_{mn} = \frac{1}{c}\int_{-h}^{-d} f_{1n}\left(z\right)\cos\lambda_m\left(z+h\right)dz.$$

In the similar way, multiplying both sides of Eq. (2.17) by $f_{2m}\left(z\right), m = 0,1,2,\cdots$ and

integrating with respect to z over $[-d, 0]$.

$$B_{lm}^{D} = \frac{\sum_{n=0}^{\infty} A_{ln}^{D} H_{mn} + \beta_l J_l(k_1 a)\Gamma_0 H_{m0}}{s_{lm}}, \quad m = 0,1,2,\cdots \tag{2.19}$$

where

$$H_{mn} = \frac{1}{d}\int_{-d}^{0} f_{1n}(z) f_{2m}(z) dz.$$

The continuity of $\frac{\partial \varphi_D^l}{\partial r}$ at $r = a$ also requires

$$\beta_l k_1 J_l'(k_1 a)\Gamma_0 f_{10}(z) + \sum_{n=0}^{\infty} A_{ln}^{D} q_{ln} \frac{f_{1n}(z)}{h} = \begin{cases} \sum_{n=0}^{\infty} B_{ln}^{D} p_{ln} \frac{f_{2n}(z)}{d}, & -d \le z \le 0 \\ 2\sum_{n=1}^{\infty} C_{ln}^{D} w_{ln} \frac{\cos\lambda_n(z+h)}{c}, & -h \le z \le -d \end{cases} \tag{2.20}$$

where

$$p_{ln} = k_{2n} d\left[I_l'(k_{2n} a) - \frac{I_l'(k_{2n} b)}{K_l'(k_{2n} b)} K_l'(k_{2n} a) \right],$$

$$q_{ln} = \frac{k_{1n} h K_l'(k_{1n} a)}{K_l(k_{1n} a)}, \; w_{ln} = \frac{\lambda_n c I_l'(\lambda_n a)}{I_l(\lambda_n a)}.$$

By multiplying both sides of Eq. (2.20) by $f_{1m}(z)$, $m = 0,1,2,\cdots$ and then integrating with respect to z over $[-h, 0]$, we obtain

$$A_{lm}^{D} q_{lm} = -\beta_l k_1 h J_l'(k_1 a)\Gamma_0 \delta_{m0} + \sum_{n=0}^{\infty} B_{ln}^{D} p_{ln} H_{nm} + 2\sum_{n=1}^{\infty} C_{ln}^{D} w_{ln} G_{nm}. \quad (2.21)$$

Using Eqs.(2.18) and (2.19), we obtain a system of equations

$$A_{lm}^{D} + \sum_{k=0}^{\infty} \frac{F_{lmk}}{q_{lm}} A_{lk}^{D} = \frac{X_{lm}^{D}}{q_{lm}}, \quad l,m = 0,1,2,\cdots \quad (2.22)$$

where

$$F_{lmk} = -\sum_{n=0}^{\infty} \frac{p_{ln} H_{nk} H_{nm}}{s_{ln}} - 2\sum_{n=1}^{\infty} w_{ln} G_{nk} G_{nm},$$

$$X_{lm}^{D} = -\beta_l k_1 h J_l'(k_1 a)\Gamma_0 \delta_{m0} + \sum_{n=0}^{\infty} \frac{p_{ln} \beta_l J_l(k_1 a)\Gamma_0 H_{n0} H_{nm}}{s_{ln}} + 2\sum_{n=1}^{\infty} w_{ln} \beta_l J_l(k_1 a)\Gamma_0 G_{n0} G_{nm}.$$

For the numerical solutions of Eq. (2.22), the series are truncated after the Nth term. Thus, we have (N+1) unknowns of A_{lm}^{D}. The unknowns constants B_{lm}^{D}, C_{lm}^{D} for the regions (II) and (III) can be determined from Eqs. (2.18) and (2.19).

From the solutions of the velocity potential, thevertical wave exciting force $F_D\left(=\mathrm{Re}\left\{X_3 e^{-i\omega t}\right\}\right)$ on the bodycan be obtained by integrating the pressure over the damping plate and the bottom of the cylinder in the region (II) and (III).

$$X_3 = 2\pi\rho g A\left[\int_0^a r\varphi_D^{0(3)}(r,-d)\,dr - \int_b^a r\varphi_D^{0(2)}(r,-d)\,dr\right]. \quad (2.23)$$

2.1.2Radiation problem

The radiation problem by the vertical oscillation of the cylinder can be solved in a similar way as the diffraction problem. The velocity potential in the region (I) can be expressed by

$$\phi_R^{(1)}(r,z)=\sum_{n=0}^{\infty}A_n^R\frac{K_0(k_{1n}r)}{K_0(k_{1n}a)}f_{1n}(z). \tag{2.24}$$

The velocity potential in the regions (II) and (III) can be written as the sum of a particular solution and a homogeneous solution.

$$\phi_R^{(2)}(r,z)=\psi_p^{(2)}(r,z)+\sum_{n=0}^{\infty}B_n^R\left(I_0(k_{2n}r)-\frac{I_0'(k_{2n}b)}{K_0'(k_{2n}b)}K_0(k_{2n}r)\right)f_{2n}(z), \tag{2.25}$$

$$\phi_R^{(3)}(r,z)=\psi_p^{(3)}(r,z)+\sum_{n=0}^{\infty}\varepsilon_n C_n^R\frac{I_0(\lambda_n r)}{I_0(\lambda_n a)}\cos\lambda_n(z+h). \tag{2.26}$$

The particular solutions in the region (II) satisfying the inhomogeneous body boundary condition can be written as follows:

$$\psi_p^{(2)}(r,z)=z+\frac{1}{K}. \tag{2.27}$$

The particular solutions in the region (III) can be written by:

$$\psi_p^{(3)}(r,z)=\frac{1}{2c}\left[(z+h)^2-\frac{r^2}{2}\right]. \tag{2.28}$$

The unknown coefficients A_n^R, B_n^R, C_n^R can be determined by invoking the continuity of potential and normal velocity at $r=a$.

$$A_m^R+\sum_{k=0}^{\infty}\frac{F_{0mk}}{q_{0m}}A_k^R=\frac{X_m^R}{q_{0m}}, \tag{2.29}$$

where

$$X_m^R=u_m-\sum_{n=0}^{\infty}\frac{p_{0n}h_nH_{nm}}{s_{0n}}-2\sum_{n=1}^{\infty}w_{0n}g_nG_{nm},$$

$$h_m=\frac{1}{d}\int_{-d}^{0}\psi_p^{(2)}(a,z)f_{2m}(z)dz,$$

$$g_m=\frac{1}{c}\int_{-h}^{-d}\psi_p^{(3)}(a,z)f_{3m}(z)dz,$$

$$u_m=\int_{-d}^{0}\frac{\partial\psi_p^{(2)}(a,z)}{\partial r}f_{1m}(z)dz+\int_{-h}^{-d}\frac{\partial\psi_p^{(3)}(a,z)}{\partial r}f_{1m}(z)dz.$$

The radiation force resulting from the forced oscillation of the body can be found by integrating the pressure multiplied by the unit normal vector over the surface of the body. For the time harmonic motion of the angular frequency ω, the radiation force $F_R\left(=\mathrm{Re}\left\{f_R e^{-i\omega t}\right\}\right)$ in a heave mode is given by

$$f_R = 2i\pi\omega\rho\left[\int_0^a r\phi_R^{(3)}(r,-d)\,dr - \int_b^a r\phi_R^{(2)}(r,-d)\,dr\right] = i\omega\left(\mu_{33} + \frac{i\nu_{33}}{\omega}\right), \quad (2.30)$$

where μ_{33} and ν_{33} are theadded mass and the radiation damping, respectively.

2.2 A circular cylinder with a rigid and a porous damping plates

We consider the diffraction and radiation problem of a circular cylinder attached with a rigid and a porous damping plates in a water depth h.The radius of the cylinder is assumed to be b and the draft to be d. The rigid damping plate with the radius a is attached at the bottom of the cylinder and the porous circular plate, the radius of which is same as the rigid one, is fixed horizontally at a depth of $d_0\ (d_0 < d)$. It is also assumed that the fluid is incompressible and inviscid, so that the fluid particle motion can be described by a velocity potential Φ. For the introduction of velocity potential, we may assume that the flow separation through the openings and irrotational wakes remain confined within a short distance of the porous plate. This means that the openings must be small and distributed uniformly. The circular cylinder for the present model is described at Fig. 2.2. Assuming the harmonic motion of the frequency ω, the velocity potential can be written as Eq. (2.1).

The potential $\phi_{D,R}$ satisfies Laplace's equation (2.2) in fluid; the free surface condition (2.3), the bottom condition (2.4), radiation condition (2.5), and the body boundary conditions Eqs. (2.6–2.7).

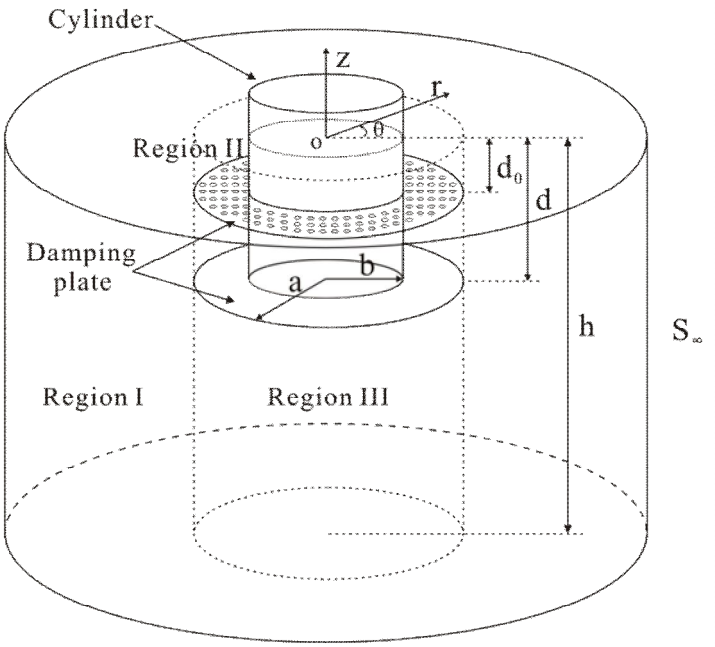

Fig.2.2. Definition sketch of the circular cylinder with dual (rigid and porous) damping plates.

To impose the boundary condition at the porous circular plate, we applied Darcy's law. As stated, the normal velocity is continuous through the porous boundary and proportional to the pressure difference between two sides of the boundary. Hence, the boundary condition on the horizontal porous plate may be written as

$$\frac{\partial \phi_{D,R}^{+}}{\partial z} = \frac{\partial \phi_{D,R}^{-}}{\partial z} = \overline{n}_{D,R} + i\sigma\left(\phi_{D,R}^{-} - \phi_{D,R}^{+}\right), \quad \text{on } z = -d_0^{\pm},\ b \le r \le a \tag{2.31}$$

where $\overline{n}_{D,R}$ denotes the normal velocity at the bottom of the cylinder ($\overline{n}_D = 0, \overline{n}_R = 1$). The superscript $\pm$ means the upper side of the porous plate and the lower side, respectively.

According to Mei et al.(1974), the imaginary part of σ is related to the inertia effect and it may be neglected when the plate is thin and the size of holes is small. The imaginary part of σ is proportional to flow accelerations, and thus has nothing to do with energy dissipation. The positive real value of σ represents viscous effects and can directly be obtained from experiments. The positive real value of σ is called the porous-effect parameter $(=\rho b_0 \omega / \mu)$ with b_0 and μ being the porosity coefficient and dynamic viscosity. The limiting case $b_0 \to 0$ corresponds to the impermeable plate and $b_0 \to \infty$ means that the plate is infinitely porous so that there is no obstruction in the fluid domain. The new dimensionless porosity parameter b_{por} used in the present numerical examples is defined as follows:

$$b_{por} = \frac{2\pi\sigma}{k_1} = \frac{2\pi\rho b_0 \omega}{k_1 \mu}. \tag{2.32}$$

After studying a systematic experimental investigation with a thin perforated steel plate in a 2-D wave tank, Cho and Kim(2008) suggested the empirical formula of $b_{por} = 57.63P - 0.9717$ where P and b_{por} where the porosity and porosity parameter, respectively.

2.2.1 Diffraction problem

To apply the MEEM, the fluid domain is divided into three regions, as shown in Fig

2.2i.e. (I) the outer region $(r \geq a, -h \leq z \leq 0)$; (II) the upper inner region of the rigid damping plate $(b \leq r \leq a, -d \leq z \leq 0)$; (III) the lower inner region of the rigid damping plate $(0 \leq r \leq a, -h \leq z \leq -d)$.

In the outer region $r \geq a$, the velocity potential satisfying Eqs. (2.2–2.5)can be written as:

$$\varphi_D^{l(1)}(r,z) = \beta_l J_l(k_1 r)\Gamma_0 f_{10}(z) + \sum_{n=0}^{\infty} A_{ln}^D \frac{K_l(k_{1n} r)}{K_l(k_{1n} a)} f_{1n}(z). \tag{2.33}$$

The eigenvalue k_{1n} in Eq. (2.33) is the solutions of the dispersion relation Eq. (2.10). The eigenfunctions $f_{1n}(z)$ in Eq. (2.33) are given at Eq. (2.11) and also satisfy the orthogonality Eq. (2.12).

In the region (II), the diffraction potential which satisfies body boundary conditions can be written as follows:

$$\varphi_D^{l(2)}(r,z) = \sum_{n=0}^{\infty} B_{ln}^D \left(J_l(k_{2n} r) - \frac{J_l'(k_{2n} b)}{H_l'(k_{2n} b)} H_l(k_{2n} r) \right) f_{2n}(z), \tag{2.34}$$

where H_l is the Hankel function of the first kind.

The eigenfunctions $f_{2n}(z)$ and eigenvalues k_{2n} in the region (II) are the actual solutions of the following boundary value problem of a function $\tilde{f}$ with parameter κ :

$$\frac{d^2\tilde{f}}{dz} - \kappa^2 \tilde{f} = 0, \tag{2.35}$$

$$\frac{d\tilde{f}}{dz} - K\tilde{f} = 0, \quad \text{on } z = 0 \tag{2.36}$$

$$\left.\frac{d\tilde{f}}{dz}\right|_{z=-d_0^+} = \left.\frac{d\tilde{f}}{dz}\right|_{z=-d_0^-} = i\sigma\left(\left.\tilde{f}\right|_{z=-d_0^-} - \left.\tilde{f}\right|_{z=-d_0^+}\right), \tag{2.37}$$

$$\frac{d\tilde{f}}{dz} = 0, \qquad \text{on } z = -d \tag{2.38}$$

for the upper complex plane of κ and $0 < \sigma < \infty$. Then, the following complex dispersion relation should be satisfied:

$$\kappa \sinh\kappa(d - d_0)\left(K\cosh\kappa d_0 - \kappa\sinh\kappa d_0\right) = i\sigma\left(K\cosh\kappa d - \kappa\sinh\kappa d\right). \tag{2.39}$$

Eq. (2.39) can be rewritten as $D(\omega,\kappa) = 0$, which is an implicit relation between the wave number κ and the frequency ω. Since $\kappa = \kappa_1 + i\kappa_2$ is a complex variable, the complex function $D(\omega,\kappa)$ can be separated by the real $\left(D_{\mathrm{Re}}(\omega,\kappa)\right)$ and imaginary part $\left(D_{\mathrm{Im}}(\omega,\kappa)\right)$. Both the real and imaginary parts are to be zero.

$$D(\omega,\kappa) = D_{\mathrm{Re}}(\omega,\kappa_1,\kappa_2) + iD_{\mathrm{Im}}(\omega,\kappa_1,\kappa_2) = 0, \tag{2.40}$$

$$D_{\mathrm{Re}}(\omega,\kappa_1,\kappa_2) = 0, \tag{2.41}$$

$$D_{\mathrm{Im}}(\omega,\kappa_1,\kappa_2) = 0. \tag{2.42}$$

With the initial guesses $\left(\kappa_1^{(0)},\kappa_2^{(0)}\right)$ of all the roots, the ordinary non-linear equation

$D(\omega,\kappa)=0$ can be easily solved by using the Newton-Raphson iteration method.

The infinite number of discrete solutions satisfying Eq. (2.39) are eigenvalues k_{2n}. The resulting eigenfunctions $f_{2n}(z)$ are

$$f_{2n}(z)=\begin{cases}\sinh k_{2n}(d-d_0)\left(k_{2n}\cosh k_{2n}z+K\sinh k_{2n}z\right), & -d_0\le z\le 0\\ \left(K\cosh k_{2n}d_0-k_{2n}\sinh k_{2n}d_0\right)\cosh k_{2n}(z+d). & -d\le z\le -d_0\end{cases} \tag{2.43}$$

By straightforward integration using Eq. (2.43), it can be shown that the eigenfunctions satisfy orthogonal relation.

$$\frac{1}{d}\int_{-d}^{0} f_{2n}(z)f_{2m}(z)dz=N_{2m}\delta_{mn}. \tag{2.44}$$

In the region (III), the diffraction potential takes the following form

$$\varphi_D^{l(3)}(r,z)=\sum_{n=0}^{\infty}\varepsilon_n C_{ln}^{D}\frac{I_l(k_{3n}r)}{I_l(k_{3n}a)}f_{3n}(z). \tag{2.45}$$

The vertical eigenfunctions and eigenvalues in Eq. (2.45) are given by

$$f_{3n}(z)=\cos k_{3n}(z+h).\ k_{3n}=\frac{n\pi}{c} \tag{2.46}$$

The continuity of φ_D^l on $r=a$ requires

$$\beta_l J_l\left(k_1 a\right)\Gamma_0 f_{10}\left(z\right)+\sum_{n=0}^{\infty} A_{ln}^D f_{1n}\left(z\right)=\begin{cases}\sum_{n=0}^{\infty} B_{ln}^D s_{ln} f_{2n}\left(z\right), & -d\le z\le 0\\ \sum_{n=0}^{\infty} \varepsilon_n C_{ln}^D f_{3n}\left(z\right), & -h\le z\le -d\end{cases} \tag{2.47}$$

where

$$s_{ln}=J_l\left(k_{2n}a\right)-\frac{J_l'\left(k_{2n}b\right)}{H_l'\left(k_{2n}b\right)}H_l\left(k_{2n}a\right).$$

If we multiply (2.47) by $f_{3m}\left(z\right)$, $m=0,1,2,\cdots$ and integrate with respect to z from $-h$ to $-d$, the following equation can be obtained.

$$C_{lm}^D=\sum_{n=0}^{\infty} A_{ln}G_{mn}+\beta_l J_l\left(k_1 a\right)\Gamma_0 G_{m0},\ m=0,1,2,\cdots \tag{2.48}$$

where

$$G_{mn}=\frac{1}{c}\int_{-h}^{-d} f_{1n}\left(z\right)f_{3m}\left(z\right)dz=\frac{\left(-1\right)^m k_{1n}\sin k_{1n}c}{N_{1n}c\left(k_{1n}^2-k_{3m}^2\right)}.$$

Multiplying (2.47) by $f_{2m}\left(z\right)$, $m=0,1,2,\cdots$ and integrating with respect to z over the region of validity $\left[-d,0\right]$.

$$B_{lm}^D=\frac{\sum_{n=0}^{\infty} A_{ln}^D H_{mn}+\beta_l J_l\left(k_1 a\right)\Gamma_0 H_{m0}}{s_{lm}N_{2m}}.\ m=0,1,2,\cdots \tag{2.49}$$

The continuity of $\frac{\partial\varphi_D^l}{\partial r}$ on $r=a$ also requires

$$\beta_l k_1 J_l'(k_1 a)\Gamma_0 f_{10}(z) + \sum_{n=0}^{\infty} A_{ln}^D q_{\ln} \frac{f_{1n}(z)}{h} = \begin{cases} \sum_{n=0}^{\infty} B_{ln}^D p_{ln} \frac{f_{2n}(z)}{d}, & -d \le z \le 0 \\ \sum_{n=0}^{\infty} \varepsilon_n C_{ln}^D w_{ln} \frac{f_{3n}(z)}{c}. & -h \le z \le -d \end{cases} \quad (2.50)$$

where

$$q_{ln} = k_{1n} h \frac{K_l'(k_{1n} a)}{K_l(k_{1n} a)},$$

$$p_{ln} = k_{2n} d \left[J_l'(k_{2n} a) - \frac{J_l'(k_{2n} b)}{H_l'(k_{2n} b)} H_l'(k_{2n} a) \right],$$

$$w_{ln} = k_{3n} c \frac{I_l'(k_{3n} a)}{I_l(k_{3n} a)}.$$

If we multiply both sides of Eq. (2.50) by $f_{1m}(z)$, $m = 0,1,2,\cdots$ and then integrate both sides from $-h$ to 0 and use the orthogonal property of the eigenfunction $f_{1m}(z)$, the following equation can be obtained.

$$A_{lm}^D q_{lm} = -\beta_l k_1 h J_l'(k_1 a)\delta_{m0} + \sum_{n=0}^{\infty} B_{ln}^D p_{\ln} H_{nm} + 2\sum_{n=1}^{\infty} C_{ln}^D w_{ln} G_{nm}, \quad (2.51)$$

If substituting Eqs. (2.48) and (2.49) into Eq. (2.51), we obtain a system of equation

$$A_{lm}^D + \sum_{k=0}^{\infty} \frac{F_{lmk}}{q_{lm}} A_{lk}^D = \frac{X_{lm}^D}{q_{lm}}, \quad (2.52)$$

where

$$F_{lmk} = -\sum_{n=0}^{\infty} \frac{p_{ln} H_{nk} H_{nm}}{s_{ln} N_{2n}} - 2\sum_{n=1}^{\infty} w_{ln} G_{nk} G_{nm},$$

$$X_{lm}^{D} = -\beta_l k_1 h J_l'(k_1 a)\Gamma_0 \delta_{m0} + \sum_{n=0}^{\infty} \frac{p_{\ln} \beta_l J_l(k_1 a)\Gamma_0 H_{n0} H_{nm}}{s_{ln} N_{2n}} + 2\sum_{n=1}^{\infty} w_{ln} \beta_l J_l(k_1 a)\Gamma_0 G_{n0} G_{nm}.$$

Eq. (2.52) is the algebraic linear equation for the unknown coefficient A_{lm}^{D}. The infinite matrix may be truncated at a certain term to solve the matrix equation numerically. By solving the above matrix equations, the unknown constants B_{lm}^{D}, C_{lm}^{D} can be determined from Eqs. (2.48) and (2.49).

The wave exciting forces can be obtained by integrating the pressure over the body surface.

$$X_3 = 2\pi\rho g A\left[\int_0^a r\varphi_D^{0(3)}(r,-d)\,dr - \int_b^a r\varphi_D^{0(2)}(r,-d)\,dr + \int_b^a r\left(\varphi_D^{0(2)}(r,-d_0^-) - \varphi_D^{0(2)}(r,-d_0^+)\right)dr\right]. \tag{2.53}$$

2.2.2 Radiation problem

In the regions (II) and (III), the radiation potential can be written as the sum of a particular solution and a homogeneous solution. Therefore, the radiation potential in each three region can be written as:

$$\phi_R^{(1)}(r,z)=\sum_{n=0}^{\infty}A_n^R\frac{K_0(k_{1n}r)}{K_0(k_{1n}a)}f_{1n}(z), \tag{2.54}$$

$$\phi_R^{(2)}(r,z)=\psi_p^{(2)}(r,z)+\sum_{n=0}^{\infty}B_n^R\left(J_0(k_{2n}r)-\frac{J_0'(k_{2n}b)}{H_0'(k_{2n}b)}H_0(k_{2n}r)\right)f_{2n}(z), \tag{2.55}$$

$$\phi_R^{(3)}(r,z)=\psi_p^{(3)}(r,z)+\sum_{n=0}^{\infty}\varepsilon_n C_n^R\frac{I_0(k_{3n}r)}{I_0(k_{3n}a)}f_{3n}(z). \tag{2.56}$$

The particular solutions in the regions (II) and (III) satisfy the inhomogeneous body boundary condition by Eqs. (2.27) and (2.28).

The unknown coefficients A_n^R, B_n^R, C_n^R can be determined by Eq. (2.29).The radiation force in the heave mode is given by

$$\begin{aligned} f_R &= 2i\pi\omega\rho\left[\int_0^a r\phi_R^{(3)}(r,-d)\,dr-\int_b^a r\phi_R^{(2)}(r,-d)\,dr+\int_b^a r\left(\phi_R^{(2)}(r,-d_0^-)-\phi_R^{(2)}(r,-d_0^+)\right)dr\right] \\ &= i\omega\left(\mu_{33}+\frac{i\nu_{33}}{\omega}\right). \end{aligned} \tag{2.57}$$

2.3 Equation of heave motion

Using Newton's second law, the equilibrium between the inertia of the structure and the external forces can be written as:

$$M\ddot{z} = F_R + F_h + F_D, \tag{2.58}$$

where $M\left(=\rho Sd\right)$ denotes the mass of the cylinder, $\ddot{z}$ the second time derivative of the heave motion of the cylinder. $F_h\left(=-\rho gS\,z\right)$ representsthe hydrostatic restoring force.

The equation of motion (2.58) can be rewritten as:

$$(M+\mu_{33})\ddot{z} + \left(B_{vis}+\nu_{33}\right)\dot{z} + \rho gS\,z = F_D, \tag{2.59}$$

where $S(=\pi a^2)$ is the water-plane area. B_{vis} is viscous damping coefficient, which is calculated from $B_{vis} = 2\kappa_d \rho gS/\omega_o$, where κ_d is the non-dimensional damping coefficient and $\omega_o\left(\approx\sqrt{\rho gS/\left(M+\mu_{33}\right)}\right)$ is the undamped natural frequency. The κ_d can be determined from the freedecay test in still water.

2.3.1 Frequency domain analysis

Considering the vertical harmonic oscillating motion of the cylinder, it is possible to

decompose each term of Eq. (2.59) in spatial and temporal dependencies. Therefore, the equation of heave motion in the frequency domain is written by:

$$\left\{-\omega^2(M+\mu_{33})-i\omega(B_{vis}+\nu_{33})+\rho gS\right\}z_a = X_3. \tag{2.60}$$

2.3.2Time domain analysis

The equation of heave motion of the cylinder in the time domain is expressed by integro-differential equation as follows (Cummins, 1962):

$$(M+\mu_{33}(\infty))\ddot{z}+B_{vis}\dot{z}+\int_0^t K(\tau)\dot{z}(t-\tau)d\tau+\rho gS\,z = F_D(t), \tag{2.61}$$

where the upper dots denote time derivatives.The integral in Eq. (2.61) is a memory term expressing the radiation wave damping, where the heave impulse response function $K(\tau)$ can be calculated by functions of buoy frequency response by the inverse Fourier transform,

$$\begin{aligned} K(\tau) &= -\frac{2}{\pi}\int_0^\infty \left(\mu_{33}(\omega)-\mu_{33}(\infty)\right)\omega\sin(\omega\tau)d\omega \\ &= \frac{2}{\pi}\int_0^\infty \nu_{33}(\omega)\cos(\omega\tau)d\omega. \end{aligned} \tag{2.62}$$

For the calculation of integral in Eq. (2.62), the entire frequency range is divided into a finite number of sub-domains and the integral can be expressed in terms of sum of integrals over N_p+1 sub-domains (ω_n,ω_{n+1}) and (ω_{N+1},∞). Then, the integral over each

sub-domain can be readily obtained by numerical integrations.

$$K(\tau) = \sum_{n=1}^{N_p} \Delta K_n(\tau) + K_\infty(\tau), \tag{2.63}$$

where

$$\Delta K_n(\tau) = \frac{2}{\pi} \int_{\omega_n}^{\omega_{n+1}} \nu_{33}(\omega) \cos(\omega\tau) d\omega,$$
$$K_\infty(\tau) = \frac{2}{\pi} \int_{\omega_{N+1}}^{\infty} \nu_{33}(\omega) \cos(\omega\tau) d\omega.$$

For the numerical calculation of $\Delta K_n(\tau)$, the radiation damping $\nu_{33}(\omega)$ is to be approximated by the linear function within sub-domains (ω_n, ω_{n+1})

$$\nu_{33}(\omega) \approx a_0 + a_1\omega, \quad \omega_n \le \omega \le \omega_{n+1} \tag{2.64}$$

where

$$a_0 = \frac{\nu_{33}(\omega_n)\omega_{n+1} - \nu_{33}(\omega_{n+1})\omega_n}{\omega_{n+1} - \omega_n},$$
$$a_1 = \frac{\nu_{33}(\omega_{n+1}) - \nu_{33}(\omega_n)}{\omega_{n+1} - \omega_n}.$$

The contribution to the impulse response function from sub-domains can be written as

$$\Delta K_n(\tau) \approx \frac{2}{\pi} \int_{\omega_n}^{\omega_{n+1}} \left(a_0 + a_1\omega\right) \cos(\omega\tau) d\omega = a_0 P_0 + a_1 P_1, \tag{2.65}$$

where

$$P_0 = \frac{2}{\pi}\int_{\omega_n}^{\omega_{n+1}} \cos(\omega\tau)d\omega = \frac{2}{\pi}\left(\frac{\sin(\omega_{n+1}\tau)-\sin(\omega_n\tau)}{\tau}\right),$$

$$P_1 = \frac{2}{\pi}\int_{\omega_n}^{\omega_{n+1}} \omega\cos(\omega\tau)d\omega = \frac{2}{\pi}\left(\frac{\omega_{n+1}\sin(\omega_{n+1}\tau)-\omega_n\sin(\omega_n\tau)}{\tau}+\frac{\cos(\omega_{n+1}\tau)-\cos(\omega_n\tau)}{\tau^2}\right).$$

The contribution ranging (ω_{N+1},∞) can be also calculated by a semi-analytical method. Since $\nu_{33}(\omega)$ should be vanish as $\omega\to\infty$, it can be approximated with an exponentially decay function

$$\nu_{33}(\omega) \approx \alpha e^{-\beta(\omega-\omega_{N+1})}, \tag{2.66}$$

where

$$\alpha = \nu_{33}(\omega_{N+1}),\ \beta = \frac{-1}{\nu_{33}(\omega_{N+1})}\frac{d\nu_{33}(\omega_{N+1})}{d\omega},$$

where β should be greater than 0 in order for $\nu_{33}(\omega)$ to vanish as $\omega\to\infty$. α and β are determined so that $\nu_{33}(\omega)$ and its first derivative is continuous at $\omega=\omega_{N+1}$. The contribution ranging (ω_{N+1},∞) is then

$$K_\infty(\tau) \approx \frac{2}{\pi}\int_{\omega_{N+1}}^{\infty} \alpha e^{-\beta(\omega-\omega_{N+1})}\cos(\omega\tau)d\omega = \frac{2\alpha}{\pi}\left(\frac{\beta\cos(\omega_{N+1}\tau)-\tau\sin(\omega_{N+1}\tau)}{\beta^2+\tau^2}\right). \tag{2.67}$$

The memory term expressing as a time convolution integral in Eq. (2.61) can be evaluated using the trapezoidal integration with an impulse response function.

$$I = \int_0^t K(\tau)\dot{z}(t-\tau)d\tau = \sum_{i=1}^{M} K(i\Delta t)\dot{z}(t-i\Delta t)\Delta t + \frac{K(0)\dot{z}(t)\Delta t}{2}. \quad (2.68)$$

At $t = t_{i+1} = (i+1)\Delta t$, Eq. (2.61) can be rewritten as follows:

$$\left(M + \mu_{33}(\infty)\right)\ddot{z}_{i+1} + B_{vis}\dot{z}_{i+1} + \int_0^{t_i} K(\tau)\dot{z}(t-\tau)d\tau + \rho g S z_{i+1} = (F_D)_{i+1}. \quad (2.69)$$

The general numerical solution of the equation of motion in time domain was proposed by Newmark and is commonly known as Newmark's β method. Assuming

$$\begin{aligned} \dot{z}_{i+1} &= \dot{z}_i + \frac{\Delta t}{2}\left(\ddot{z}_i + \ddot{z}_{i+1}\right), \\ z_{i+1} &= z_i + \Delta t\dot{z}_i + \left(\frac{1}{2} - \beta\right)(\Delta t)^2\ddot{z}_i + \beta(\Delta t)^2\ddot{z}_{i+1}. \end{aligned} \quad (2.70)$$

We obtain for $\beta = 1/4$ the constant average acceleration; $\beta = 1/6$ the linear average acceleration $\beta = 0$ the central difference formula.

Substituting the expression for $\dot{z}_{i+1}, z_{i+1}$ into Eq. (2.69), we obtain

$$\begin{aligned} \left[M + \mu_{33}(\infty) + B_{vis}\Delta t/2 + \rho g S\beta(\Delta t)^2\right]\ddot{z}_{i+1} &= -\left(B_{vis}\Delta t/2 + \rho g S\left(\frac{1}{2} - \beta\right)(\Delta t)^2\right)\ddot{z}_i \\ &\quad -\left(B_{vis} + \rho g S\Delta t\right)\dot{z}_i - \sum_{i=1}^{M} K(i\Delta t)\dot{z}(t_i - i\Delta t)\Delta t - \rho g S z_i + (F_D)_{i+1i}. \end{aligned} \quad (2.71)$$

Eq. (2.71) allows to compute $\ddot{z}_{i+1}$ in terms of the known quantities $(F_D)_{i+1}$, $\ddot{z}_i$, $\dot{z}_i$, z_i and $\dot{z}_{i+1}$, z_{i+1} are then computed from the Eq. (2.70). Assuming that sea-state is made of the superposition of linear periodic waves of amplitude ζ_n and the frequency ω_n with energy density represented by the frequency spectrum $S_\zeta(\omega)$, the heave exciting force can

be expressed as

$$F_D(t) = \sum_{n=1}^{N_w} \left| \frac{X_{3n}}{\zeta_n} \right| \zeta_n \cos(\omega_n t + \chi_n + \phi_n), \text{ with } \zeta_n = \sqrt{2S_\zeta(\omega_n)\Delta\omega} \quad (2.72)$$

where χ_n is a specified set of random phase $[0, 2\pi]$, and $(|X_{3n}/\zeta_n|, \phi_n)$ are the modulus and phase angle of the heave exciting force acting on buoy by a wave of unit amplitude and the frequency ω_n.

Chapter 3

DISCRIPTION OF EXPERIMENT

3.1 Free decay test

3.1.1 Introduction

The viscous damping ($B_{vis} = 2\kappa_d \rho g S / \omega_o$) iscalculated from the non-dimensional damping coefficient(κ_d)byaheave free decay test in still water.

The typical time historymotion of a free decay test is shown in Fig. 3.1. The non-dimensional damping is obtained from two successive positive or negative maximum displacements, z_{a_i} and $z_{a_{i+2}}$. However, to avoid spreading in the successively determined κ_d, caused by a possible zero–shift of the measuring signal, double amplitudes can be used as follows (Journée and Massie, 2001):

$$\kappa_d = \frac{1}{2\pi} \ln \left\{ \frac{z_{a_i} - z_{a_{i+1}}}{z_{a_{i+2}} - z_{a_{i+3}}} \right\} \tag{3.1}$$

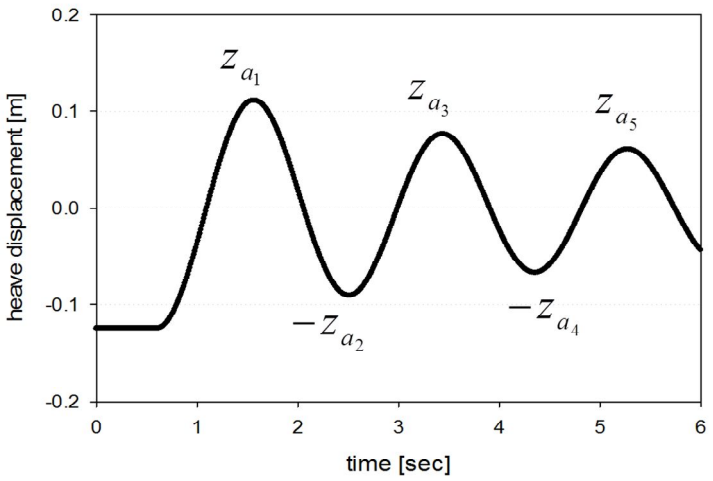

Fig.3.1. Time history of heave motion by a heave free decay test.

In this study, the initial draft of the model for the free heave oscillation was positioned by the weight on the top of the cylinder. Then, the model was oscillated at the heave natural frequency by snatching the weight. Fig. 3.2 shows the equivalent and initial positions of the cylinder with dual rigid damping plates.

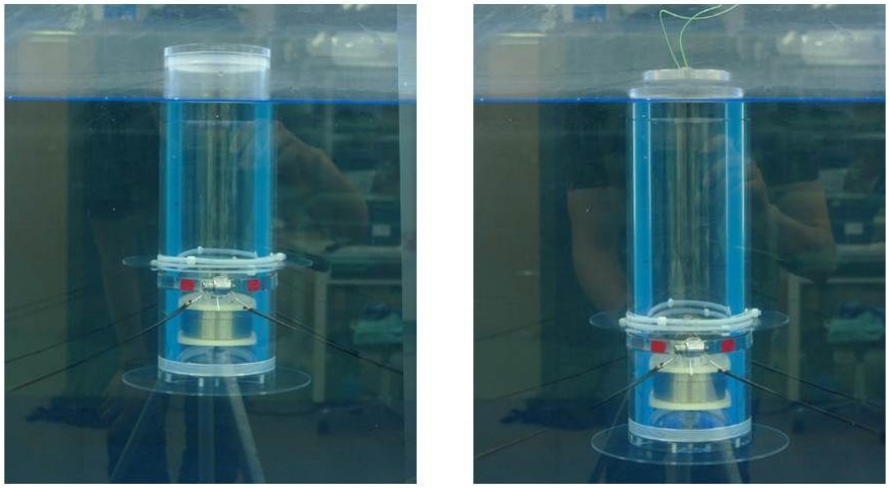

(a) (b)

Fig.3.2. The position of the cylinder with dual rigid damping plates for the heave free decay test in steel water. (a) equivalent position, (b) initial position with the 560g weight.

3.1.2Experimental set-up

The objective of the experiment was to investigatehow the damping plate as a motion reduction device affected the heave motion of the circular cylinder.Therefore, the geometry of experimental model was designed by fallingthe heave natural frequency into frequency range which the wave maker at a 2-D wave flume is capable to generate. In addition, the draft and center of mass of the model could be controlled by the weights installed at the inside bottom of the cylinder.The designed model is 0.12m in diameter and has a height of 0.353m(see Fig. 3.3).Thespecification of the experimental model aresummarized in Table 3.1.

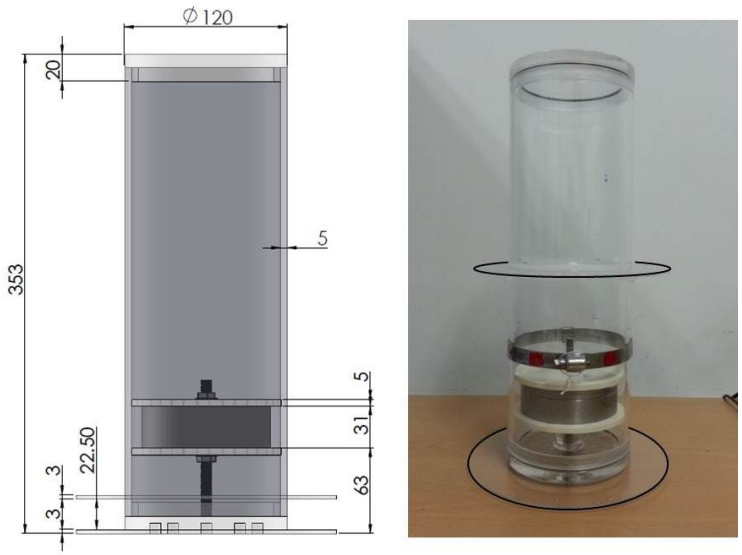

Fig.3.3.The experimental model.(a) 3D drawing, (b) fabricated shape.

Table 3.1.The specification of the experimental model.

Properties		cylinder	cylinder with a single plate	cylinder with dual plates
height (m)		0.353	-	-
diameter (m)		0.120	-	-
mass (kg)		2.890	2.9462	3.010
draft (m)		0.261	0.262	0.263
center of gravity (m)		z : -0.161	z : -0.162	z : -0.163
moment of inertia	I_{xx}, I_{yy}	0.0271	0.0279	0.0283
($kg \cdot m^2$)	I_{zz}	0.0051	0.0054	0.0056

The experimental setup is schematicallyrepresented in Fig. 3.4. Experimentshave been carried out in the 2-D wave flume at JejuNational University. The wave flume is 20.0m long, 0.8m wide, and 1.0m deep. It is usually filled with 0.6m of water.The wave was generated by a piston-type wave maker installed at one end, and an inclined porous plate wave absorber at the other end was used to reduce the reflection (see Fig. 3.5). The vision tracking system was used to capture the motion of the model. The images were recorded by a digital camera at 240 frames per second. The camera is used as a tracking device, and two red markers on the cylinder as target were on a level with the center of gravity (CoG) of the model (see Fig. 3.6). To prevent the model from drifting, it was moored loosely by four thin rubber mooring lines, as shown in Figs. 3.7 and 3.8. The body parts of the mooring lines connected the CoG and the shafts on the same height of the CoG.

In order to consider the effect of the diameter, position, and porosity of the damping plate attached on the cylinder, the experimental parameters were selected by diameter ratio (a/b), depth ratio (d_0/d), and porosity (P) of the upper-damping plate, as tabulated in Table 3.2 (see Fig. 3.9). The lower damping plate was fixed at the bottom of the cylinder.

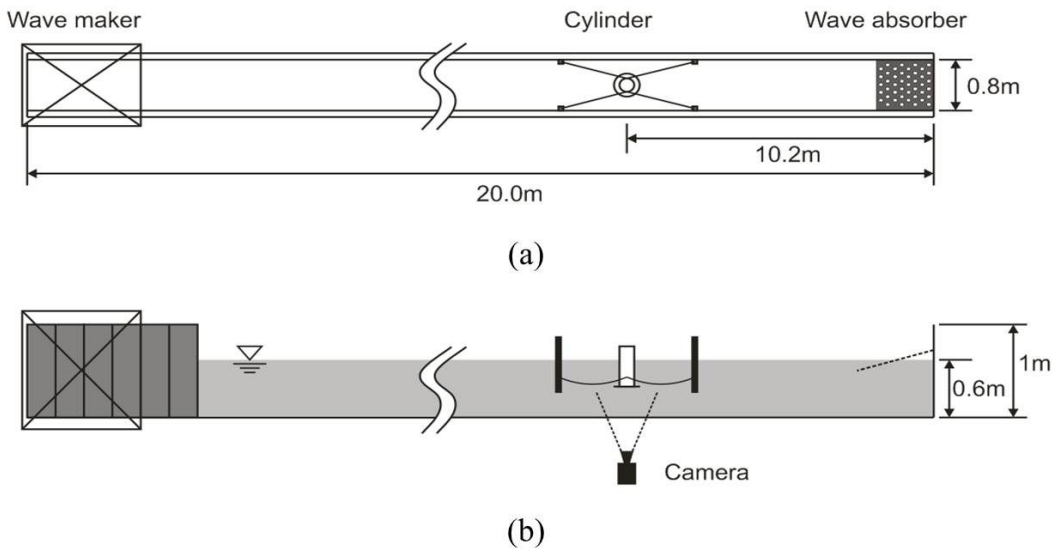

Fig.3.4. Schematic sketch of the heave free decay test setup. (a) plane view, (b) elevation view.

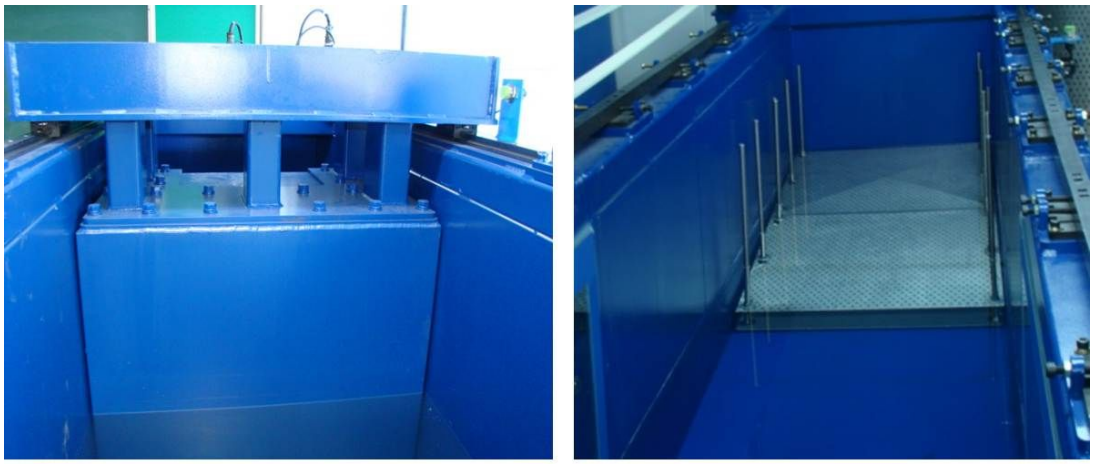

Fig.3.5. Wave generating system of the JNU wave tank. (a) piston-type wave maker, (b) inclined porous plate wave absorber.

(a) (b)

Fig.3.6.Vision tracking system. (a) targets of the model, (b) camera

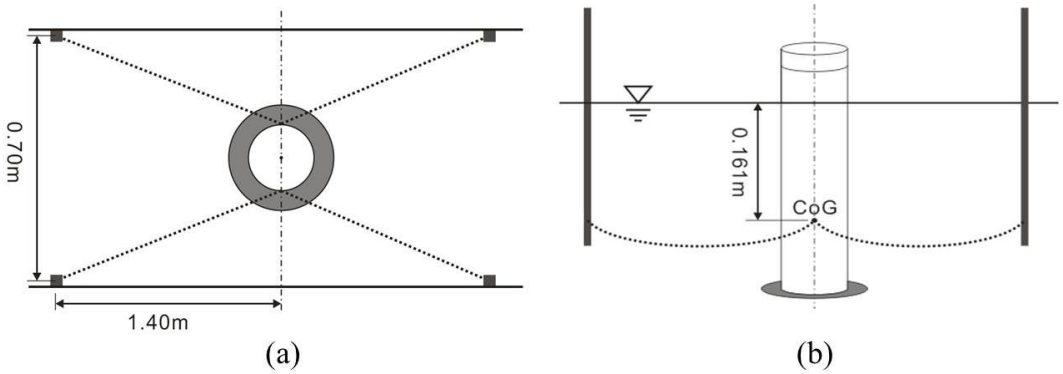

(a) (b)

Fig.3.7.Mooring configuration of the experimental model. (a) plane view, (b) elevation view.

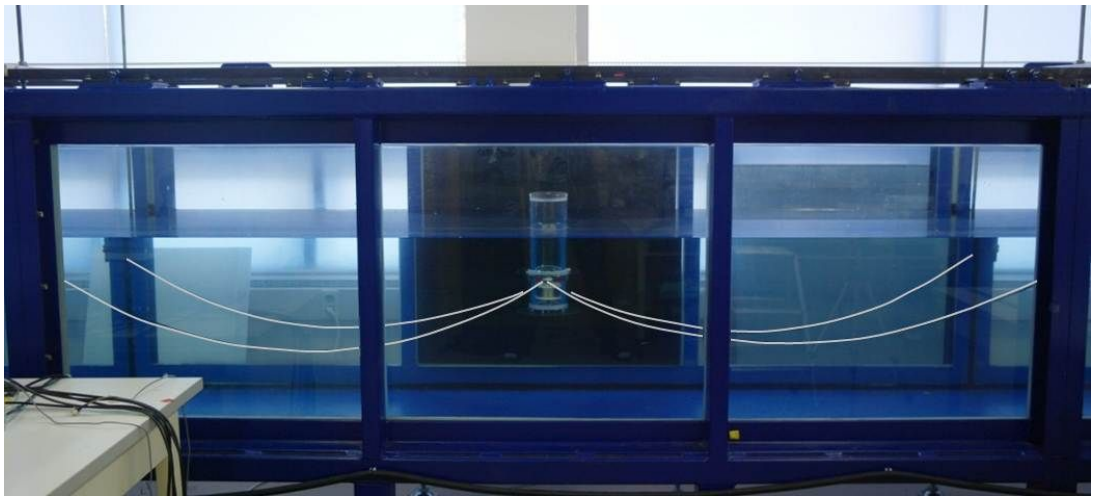

Fig.3.8.Theexperimental model installed in the JNU wave tank.

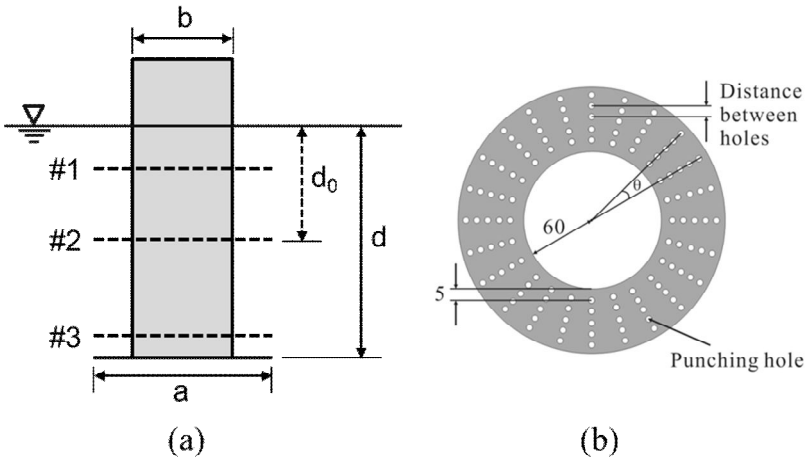

Fig.3.9. Schematic drawings for the parameter selection of the damping plate attached on the experimental model. (a) position and diameter ratio, (b) porosity of the upper-plate.

Table 3.2. Experimental parameters in the free decay test.

- depth ratio (d_0 / d) (position of a upper-plate)	0.31 (1)	0.54 (2)	0.91 (3)		
- diameter ratio (a / b) (porosity: 0.10)	1.2	1.4	1.6	1.8	
- porosity of upper-plate	0.00	0.08	0.10	0.12	0.14

3.2 Model test in regular waves

3.2.1Introduction

The purposes of model test in regular waves were to investigate the heave motion response by the damping plate at individual frequencies of the incident waves and to confirm the analytic solutions. The experiments were conducted with selected model–damping plate combinations as follow:

- cylinder only
- cylinder with a single rigid damping plate with diameter ratio (a/b) of 1.6
- cylinder with dual rigid damping plates with a/b of 1.6
- cylinder with a rigid and a porous(P =0.1) damping plate with a/b of 1.6

In case of dual damping plates, the testshave also been carried out for three positions of the upper-damping plate depending on the depth ratio (d_0/d).

3.2.2Experimental set-up

The conditions of all experimental setups were identical with the free decay test, other than generating and measuring regular waves(see Fig. 3.10). The regular waves were

generated and dissipated by the wave maker and wave absorber, respectively,either end of the 2-D wave tank. Measuring of wave elevation was undertaken using a capacitance-type wave gauge placed 4.5m from the wave maker (see Fig. 3.11). The wave frequency varied from 4.0 to 6.6rad/s to cover the heave natural frequencies for the four types of the experimental models.In addition, the wave heights were selected by the wave steepness from 0.01 to 0.02 in normal sea conditions (see Table 3.3).

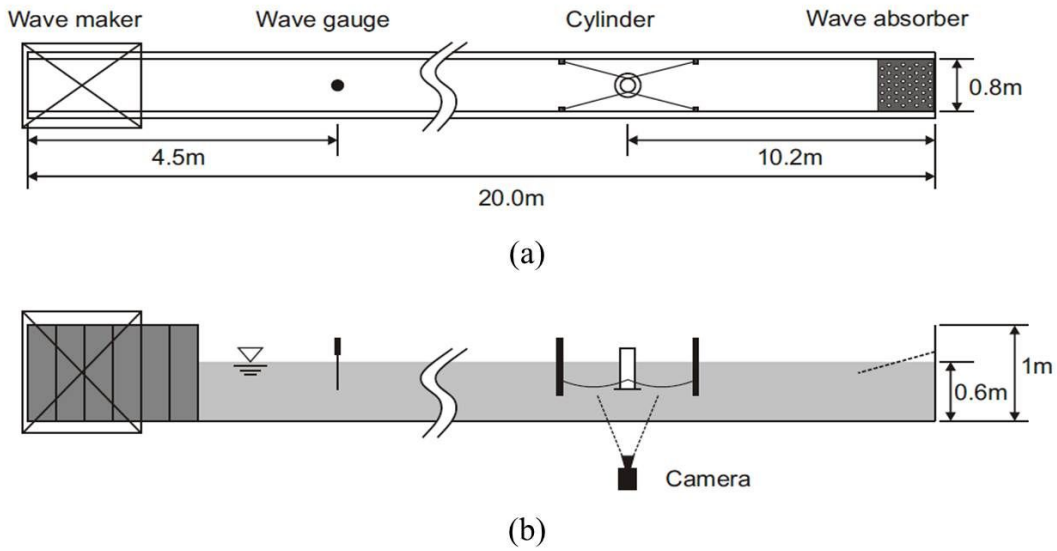

Fig.3.10. Schematic sketch of the regular wave test setup. (a) plane view, (b) elevation view.

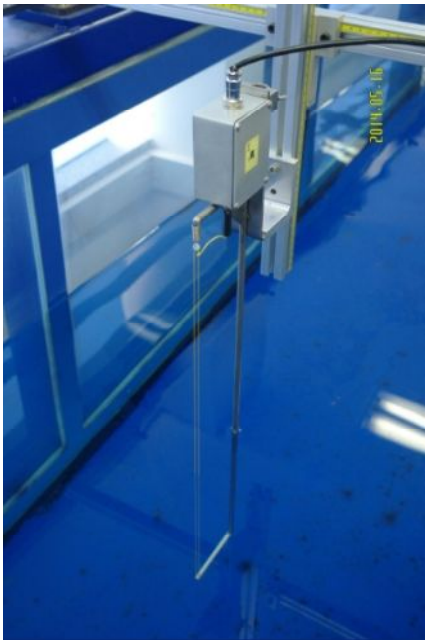

Fig.3.11.Capacitance-type wave gauge installed on the JNU wave tank.

Table 3.3. The regular wave conditions

	frequency [rad/sec]	steepness
cylinder only	4.4 ~ 6.6	0.01 ~ 0.02
cylinder w/ a single plate		
cylinder w/ dual plates	4.0 ~ 6.0	

3.3 Model test in irregular waves

3.3.1 Introduction

The objectives of model test in irregular waves were to investigate the heave motion reduction by the damping plate in the simulated real sea conditions and to confirm the time domain analytic solutions.To obtain meaningful statistical results from the test, long term measurement is required.Therefore, the long wave flume was employed to minimize the effect of the wave reflection by the length limitation of the 2-D wave flume. The experiments were carried out with two selected models-the circular cylinder only and the cylinder with a solid single damping plate with the diameter ratio (a/b) of 1.6–in a large scaled wave flume.

3.3.2Experimental set-up

The experimental model was designedfor the heave natural frequency to be included in the frequency range of a wave generating system installed at the large scaled wave flume. The designed model is 0.15m in diameter and its total height is 1.0m (see Fig. 3.12). The draft is 0.771m for the cylinder, and 0.811m for the cylinder with a damping plate. The

specification of the experimental model is summarized in Table 3.4.

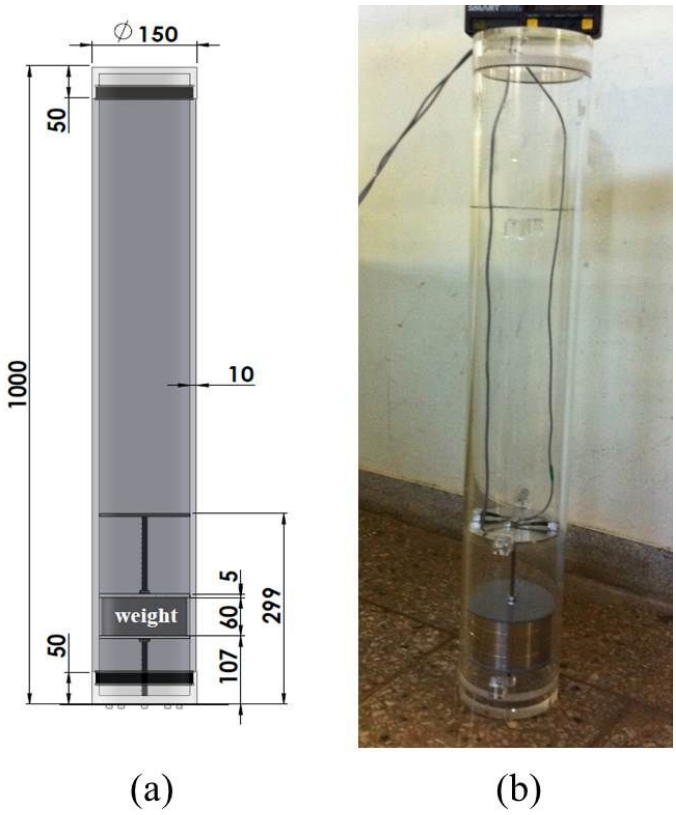

Fig.3.12.The experimental model for the irregular wave test. (a) 3D drawing, (b) fabricated model.

Table 3.4.The specification of the experimental model for model test in irregular waves.

Properties		cylinder	cylinder with damping plate
height (m)		1.000	-
diameter (m)		0.150	-
mass (kg)		13.617	14.337
draft (m)		0.771	0.811
center of gravity (m)		z : -0.413	z : -0.528
moment of inertia ($kg \cdot m^2$)	I_{xx}, I_{yy}	0.942	1.005
	I_{zz}	0.041	0.046
viscous damping coefficient		4.717	14.059

A schematic sketch of the large scaled water flume with the experimental model is depicted in Fig. 3.13. The irregular wave tests were carried out in thelarge scaled wave flume at Seoul National University. The length, width and water depth of the wave flume are 110m, 8m, and 3.5m, respectively.The eight divided plunger-type wave maker is equipped at the front of the flume and the beach type wave absorber using rubber mat is installed at the end (see Fig. 3.14). The experimental model was positioned in the center hole of the towing

carriage with four slack mooring lines using flexible spring (see Figs. 3.15 and 3.16). Both ends of the mooring lines were connected at the level of the CoG of the model. Acceleration was measured by two accelerometers placed on the CoG of the cylinder and located along the direction of the wave incidence (see Fig. 3.17 (a)). The signals of accelerometers were integrated twice to obtain the heave displacements of the model. The surface elevations were recorded with a surbo-type wave gauge (see Fig. 3.17 (b)). The irregular waves were generated with a JONSWAP spectrum with peak wave frequencies from 2.6 to 3.6rad/s and significant wave height up to 0.12m (see Table 3.5).

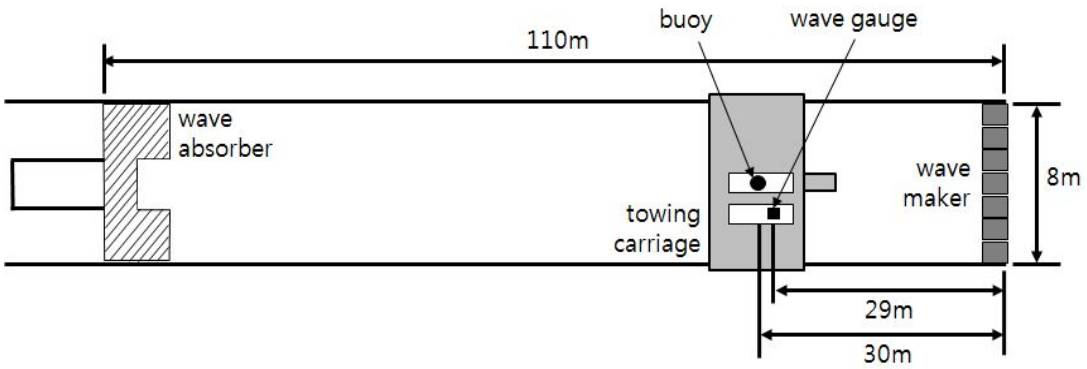

Fig.3.13. Schematic sketch of the irregular wave test setup.

(a) (b)

Fig.3.14.Wave generating system of the SNU wave tank.(a) plunger-type wave maker, (b) beach-type wave absorber.

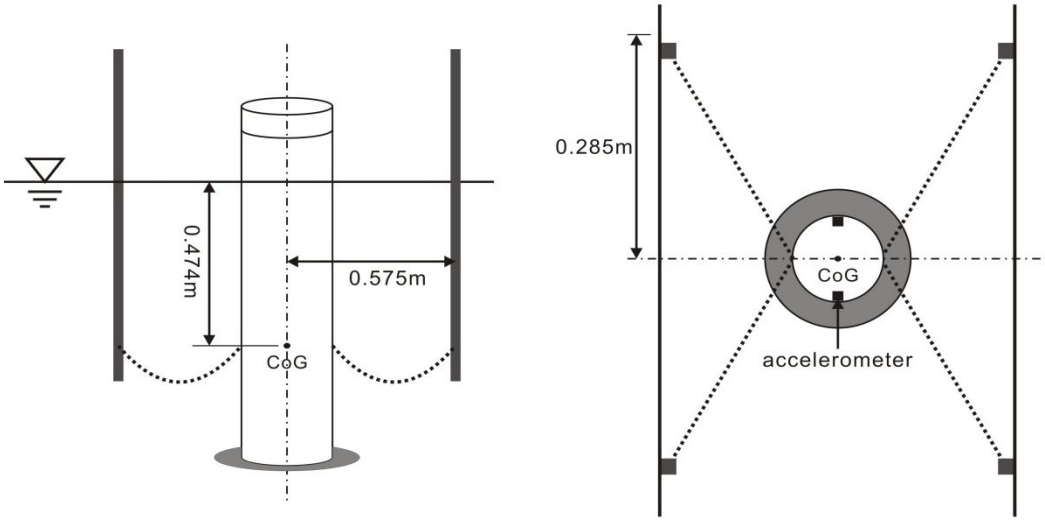

Fig.3.15.Mooring configuration of the experimental model for the irregular wave test.

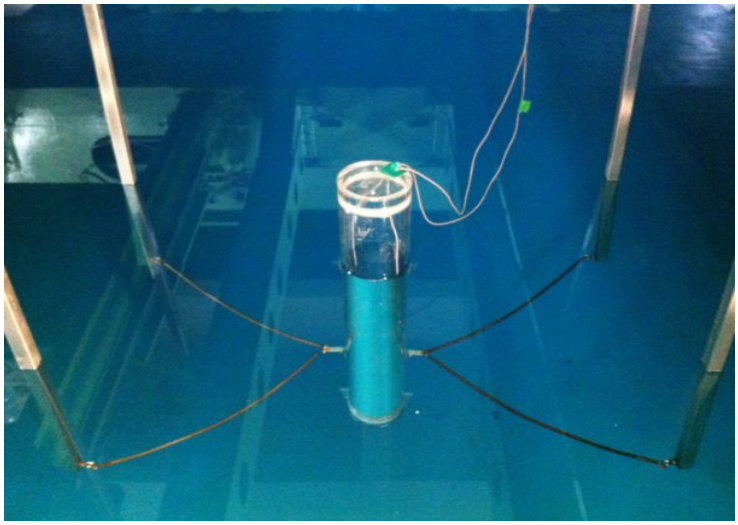

Fig.3.16. The experimental model installed in the SNU wave tank.

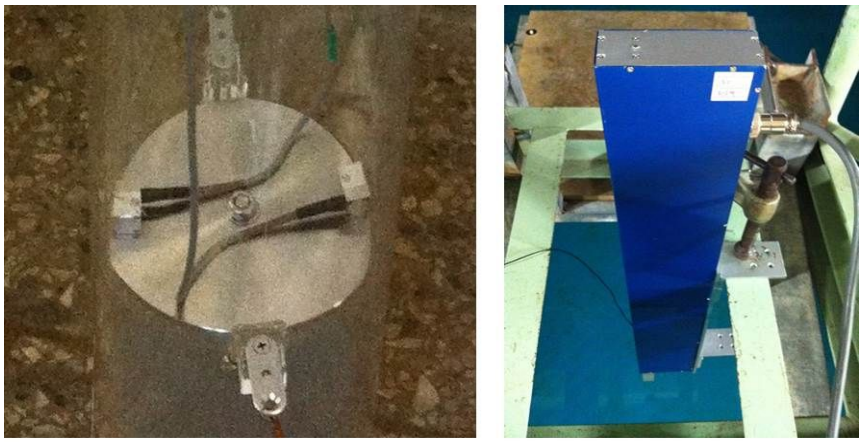

(a) (b)

Fig.3.17.Measurement system. (a) accelerometer(AS-1GB), (b) surbo-type wave gauge.

Table 3.5.The irregular wave condition.

Case		Peak frequency [rad/s]		Significant wave height [m]	
		Target	Measured	Target	Measured
cylinder only	101	3.600	3.5418	0.096	0.0915
	102	3.400	3.4582	0.107	0.0969
	103	3.200	3.1912	0.120	0.1051
	104	3.000	3.0157	0.102	0.0966
	105	2.900	2.8399	0.110	0.1041
cylinder with a single damping plate	201	3.400	3.4582	0.096	0.0872
	202	3.200	3.1912	0.108	0.1003
	203	3.000	3.0191	0.102	0.0959
	204	2.800	2.8415	0.117	0.1131
	205	2.600	2.6594	0.108	0.1054

Chapter 4

RESULTS AND DISCUSSION

4.1Introduction

In previous chapters, the mathematical formulation and the experimental setup were described for this study. In this chapter, the validation of the analytic solution is examined for the cylinder with single and dual damping plates. Discussion on the effects of the damping plate is presented based on the results of the heave free decay test.In addition,the comparisons of analytic results with experimental data are provided, focusing onthe heave motion responseof the cylinder as function of the parametric variation of the depth ratio and the porosity of the damping plate.

4.2 Comparisons

In order to verify the analytical solution derived in this research, it is compared with the experimental and numerical results (Sudhakar and Nallayarasu, 2013).The experimental model of Sudhakar and Nallayarasu (2013) (the S&N model) was scaled down to 1:100 from a prototype classic spar designed for a water depth of 300m (see in Fig. 4.1). The diameter of the rigid damping plateswas 1.3 times larger than the hull diameter of the S&N model, andthe distance between plates was fixed at 0.1625m in the case of the dual rigid damping plates. The properties of the S&N model are summarized in Table. 4.1.

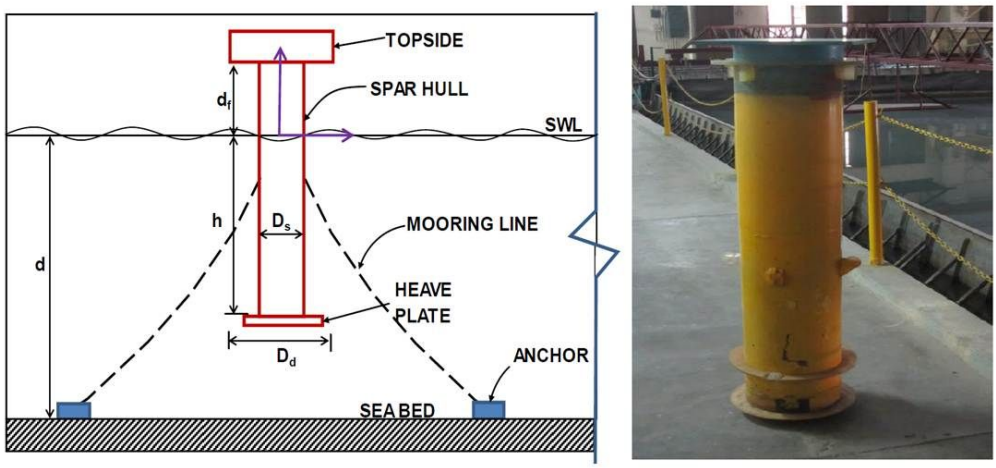

Fig.4.1. The S&N model. (a) definition sketch, (b) fabricated model.

Table 4.1.The specifications of the S&N model.

Properties		prototype	scale model (1:100)
water depth (m)		300	3
draft (m)		110	1.1
diameter (m)		25	0.25
weight (kN)		71613	71.62
buoyancy force (kN)		542944	543
center of gravity (m)		z : -49.99	z : -0.5
radius of gyration(m)	R_{xx}, R_{yy}	-	0.7907
	R_{zz}	-	0.1015
viscous damping coefficient (kg/s)		-	single plate: 30.89 dual plates: 34.32

Fig. 4.2 and Fig. 4.3 show the comparisons of analytical, numerical, and experimental results ofthe S&N model with single and dual rigid damping plates. The analytical solutions showed good agreement with both numerical and experimental results by Sudhakar and Nallayarasu (2013).

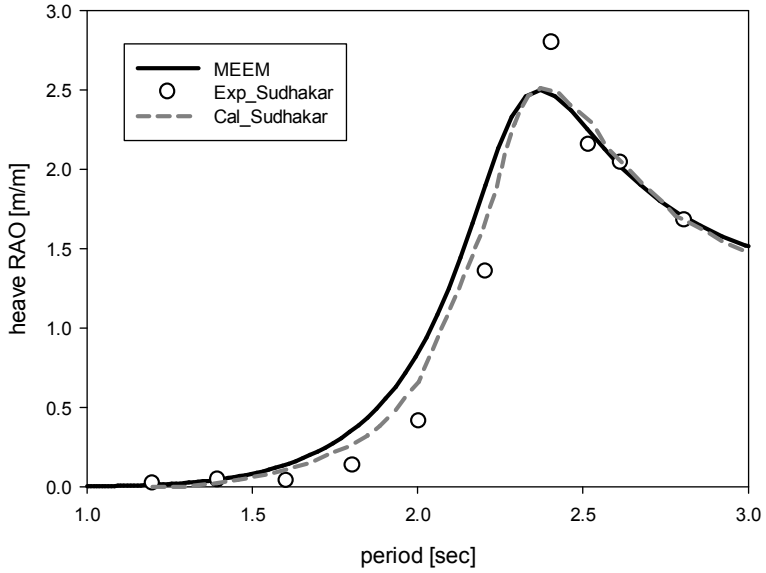

Fig.4.2.Comparison of heave RAO of classic spar with a single damping plate from MEEM with experimental and numerical results (Sudhakar and Nallayarasu, 2013).

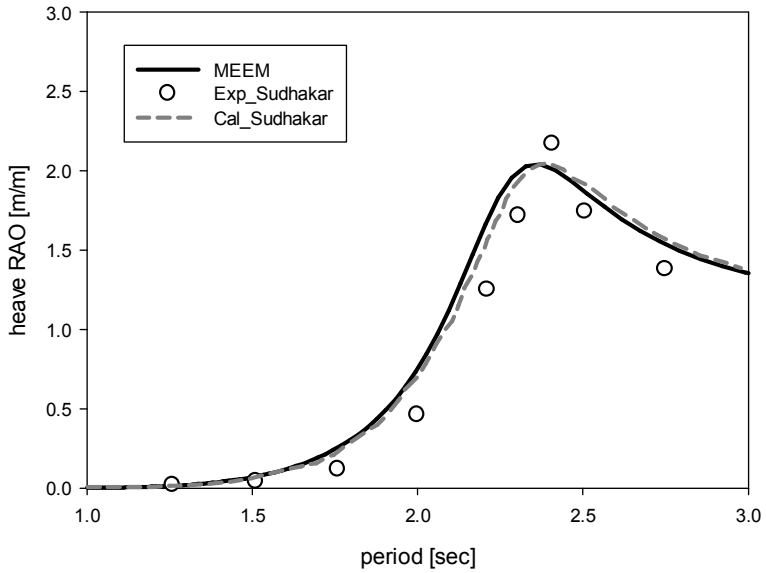

Fig.4.3. Comparison of heave RAO of classic spar with dual rigid damping plates from MEEM with experimental and numerical results (Sudhakar and Nallayarasu, 2013).

In Figs. 4.4–4.6, the hydrodynamic force (added mass, radiation damping) and wave exciting force of the S&N model with dual rigid damping plates as function of the porosity of the upperplate are presented. Since the ANSYS AQWA cannot analyze the porous effect of damping plate, the comparison between MEEM and AQWA is limited at the rigid plate. The results of MEEM in Figs. 4.4–4.6 corresponded to the numerical results obtained from the ANSYS AQWA. As the porosity was increased, the added mass tended to decrease. The decrease of the added mass due to the porosity was pronounced in the high frequency regionmore than in the low frequency region. On the contrary, the radiation damping wasincreased as the porosity was increased because the porosity parameter (b_{por}) included viscous effect by the holes of the platewas adopted to calculate the porous-effect parameter (σ). In the lower frequency region, it showed a slight increase with the porosity, while it was increased drastically in the higher frequencyregion. In contrast with the added mass or radiation damping, the variation of the porosity hardly affected the wave exciting force.

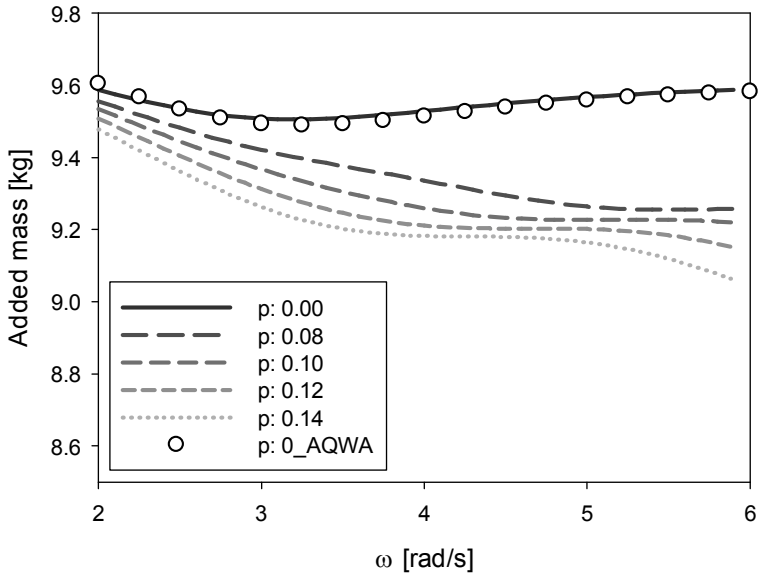

Fig.4.4. Heave added mass due to an oscillating classic spar with dual damping plates according to the porosity of the upper-damping plate.

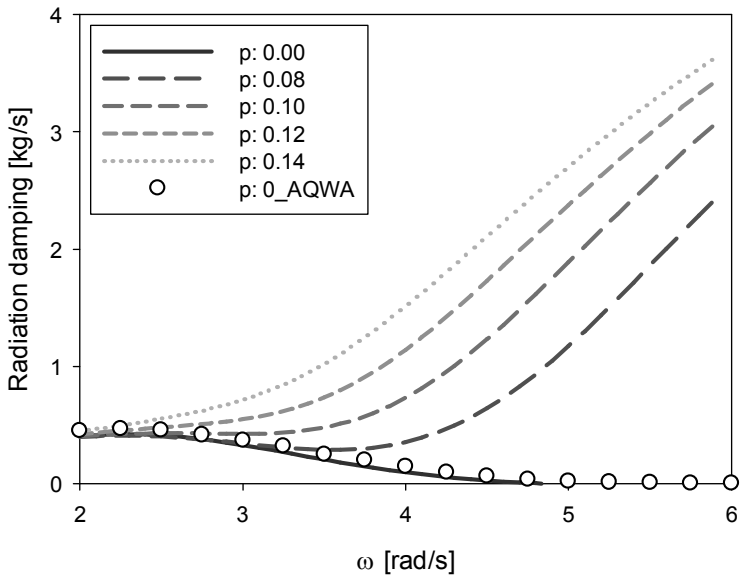

Fig.4.5. Heave damping coefficient due to an oscillating classic spar with dual damping plates according to the porosity of the upper-damping plate.

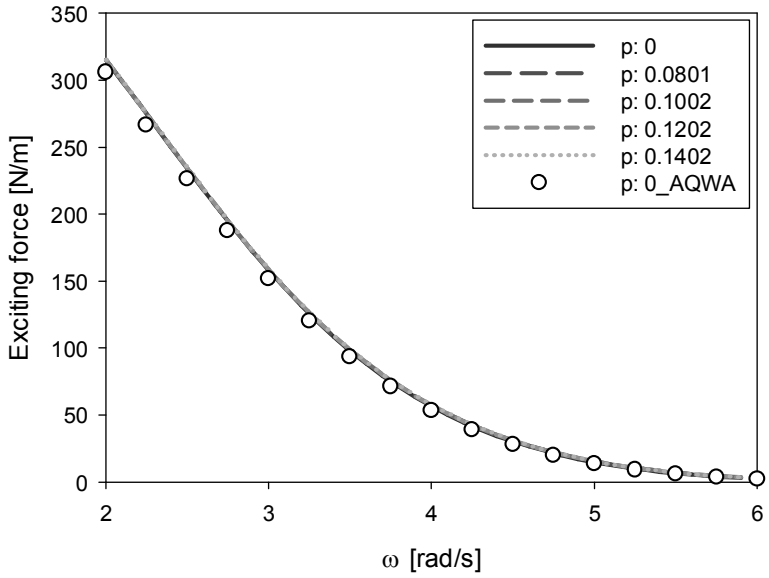

Fig.4.6. Heave wave exciting force on the classic spar with dual damping plates according to the porosity of the upper-damping plate.

4.3Free decay test

Figs. 4.7 and 4.8 show the result of the non-dimensional damping coefficient (κ_d)according to the porosity of the upper plate and the diameter of the damping plates, respectively. The black rectangle represents the result of position 1, the gray circle that of position 2, and the white inverted triangle that of position 3. The non-dimensional damping coefficients at positions 1 and 2 were nearly identical to each other, but larger compared to the damping coefficient at position3. This is because the water is trapped between the two plates in case of position 3, and thus the two plates and the trapped water physically performs as one thick damping plate (Tao et al., 2007). That is why the damping coefficient tends to be comparable where the plates are more than a specific distance apart. Furthermore, the damping coefficient of dual damping plates at position 3was even smaller than a single damping plate, as the thicker edges of the damping plate restrains the vortex formation (Tao and Cai, 2004). With regard to the variation of the porosity, the largest damping coefficient appeared at the porosity of 0.1. However, the closer the damping plate was positioned to the water surface, the smaller the effect of the porosity.

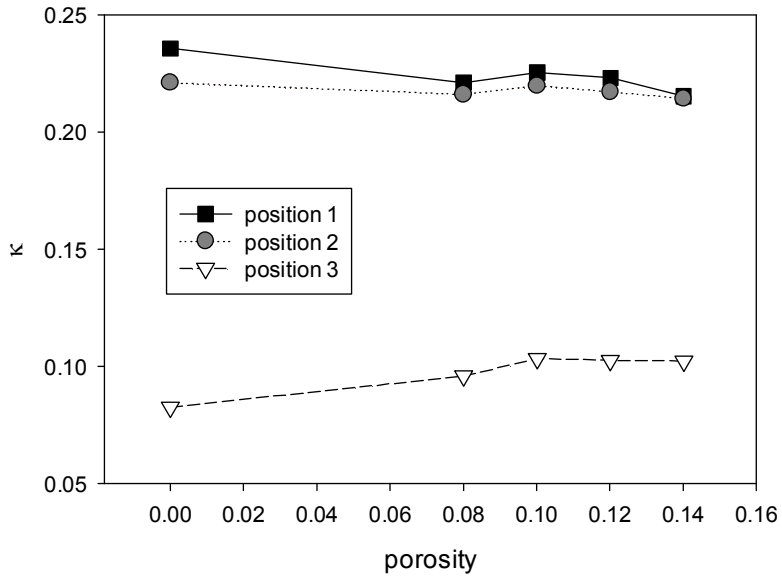

Fig.4.7.Non-dimensional damping coefficients from the free decay test as function of porosity and depth ratio for diameter ratio (a / b = 1.6).

When it comes to the free decay test depending on the variation in the diameter, the upper-damping plate with porosity of 0.1 was used (see Fig.4.8). As the diameter of the damping plate became bigger, the viscous damping tended to increase. When the diameter ratio was smaller than 1.6, the damping coefficient dramatically increased whereas under other circumstancesit showed only a slight increase tendency. This is because the vortex formation is constrained due to the correlation between the damping plates and the cylinder when the diameter ratio is small. On the other hand, for more than a specific diameter ratio, the mechanism of the vortex formation is independent from the cylinder and, therefore, no effect occurs (Tao and Cai, 2004). Consequently, the characteristics of the viscous damping

in the case of the dual damping plates are considerably affected by the position of the upper-damping plate and the diameter ratio.

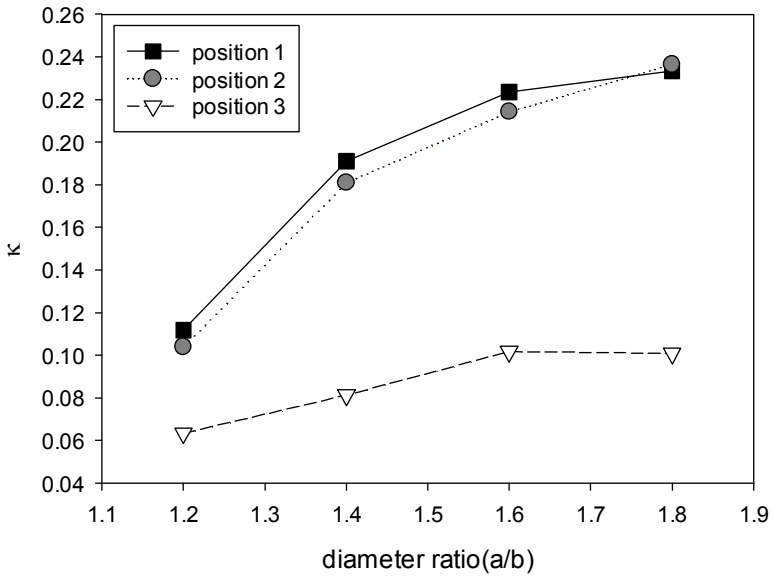

Fig.4.8.Non-dimensional damping coefficients from the free decay test as function of diameter and depth ratio for porosity ($P = 0.1$).

4.4Heave motion response in regular waves

Theheave motion testof the circular cylinder in regular waves wasprocessed to obtain the heave response amplitude operators (RAOs).Figs. 4.9 and 4.10 show the comparisons of the analytical,experimental, and numerical results. The circle represents the numerical results from ANSYS AQWA, the inverted triangle is for the experimental results, and the solid line is for the analytic solutions.The experiment results were in good agreement with all calculation results, as shown in Figs. 4.9 and 4.10. The heave RAO at the resonant frequency was more than 4 in case of using cylinder only (Fig. 4.9), but the RAO at the resonant frequency was reduced to less than 1.8 by attaching the single damping plate at the bottom of the cylinder. Since the added mass was increased by the attached damping plate, the resonant frequency shifted to the lower frequency region. In Fig. 4.9, the small peak value in the experiment results appears at 5.0rad/s, which coincides with the resonant frequency of the pitch mode. This is considered to be due to the nonlinear interaction with pitch motion.

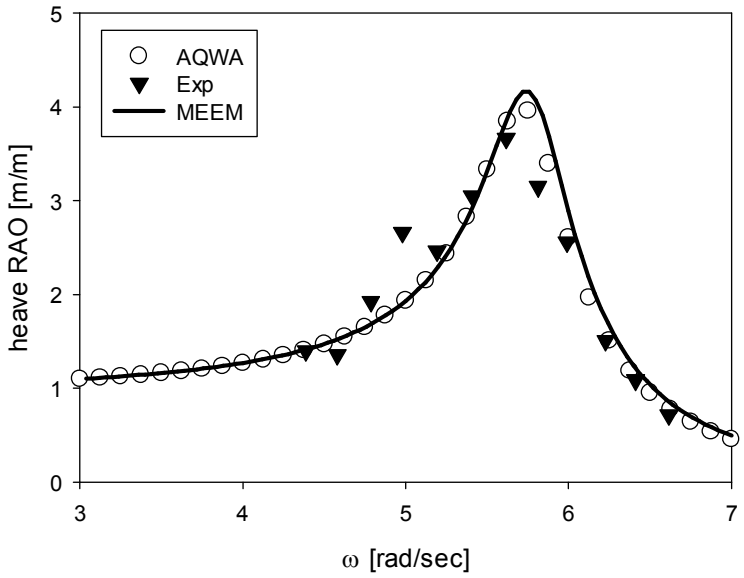

Fig.4.9. Comparison of heave RAO among analytic (MEEM), numerical (AQWA), and experimental (Exp) results in case of cylinder only (a / b =1.6).

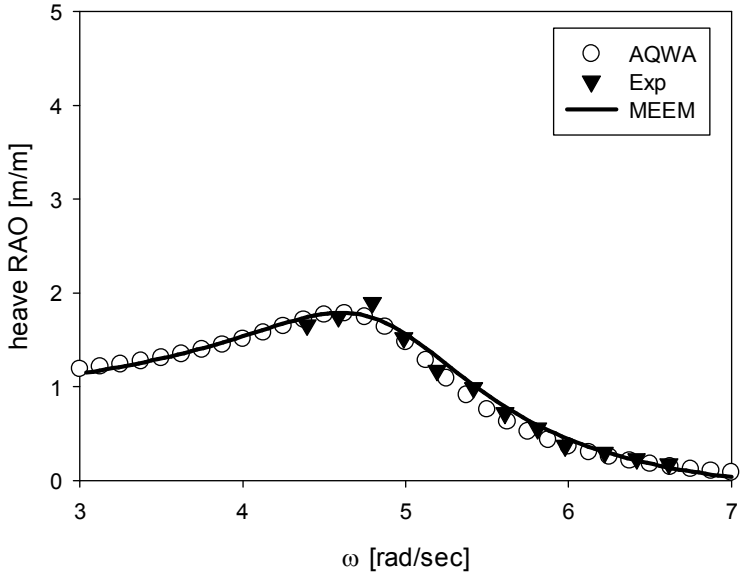

Fig.4.10. Comparison of heave RAO among analytic (MEEM), numerical (AQWA), and experimental (Exp) results in case of cylinder with a single plate attached at the bottom of the circular cylinder (a / b =1.6).

The calculated and measured results of the heave RAO of the cylinder with dual rigid damping plates as function of depth ratios of the upperplate are shown in Fig. 4.11. The colors identify the position of the upperplate: 1 (red), 2 (blue), 3 (black). All lines are the MEEM solutions, and symbols are for experimental results. Those two results were in good agreement over all frequencies. The heave RAO in the case of position 3 was apparently higher than in those of 1 and 2, as well as in the case of the single damping plate. Positions 1 and 2 showed nearly similar heave RAO curve. This tends to be the same as the results in the free decay test.

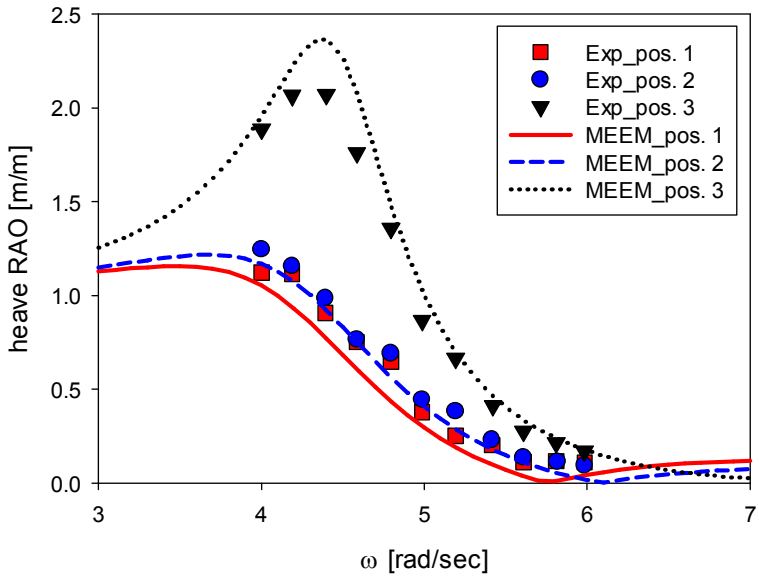

Fig.4.11. Comparison of heave RAO between analytic (MEEM) and experimental (Exp) results in case of cylinder with dual rigid damping plates for different depth ratios of the upper-damping plate (a / b =1.6).

Fig. 4.12 presents the results of the dual damping plates when the porosity of the upper-damping plate is 0.1. The effect of the porous damping plate was slight with the exception of position 3, since it was already overdamped by the dual damping plates.

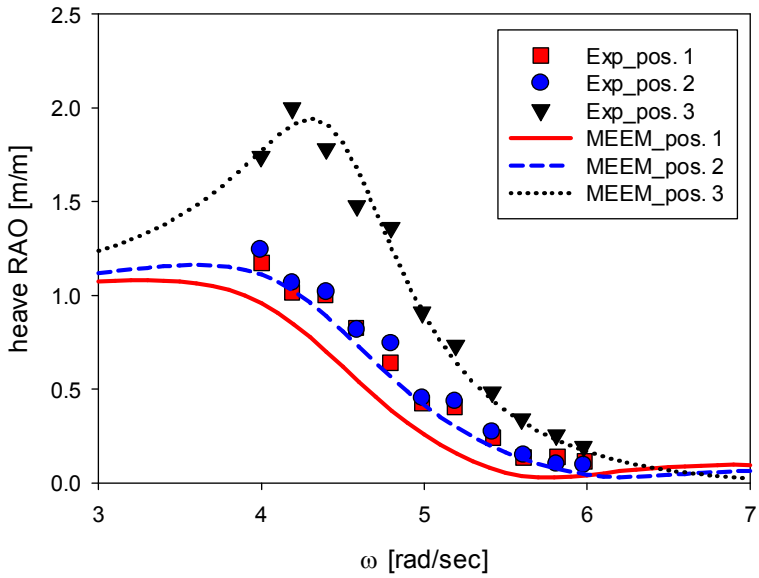

Fig.4.12. Comparison of heave RAO between analytic (MEEM) and experimental (Exp) results in case of cylinder with dual damping plates for different depth ratio of the porous (P =0.1) upper-damping plate (a / b =1.6).

The calculation results of the heave RAO depending on the variation in the porosity of the upper-damping plate of each position are shown in Figs. 4.13, 4.14, and 4.15, respectively. In the case of position 3, the smallest heave RAO is presented at P =0.1.However, in the case of position 1 and 2, the effect of the porosity hardly existed

because it was already overdamped, as mentioned above.

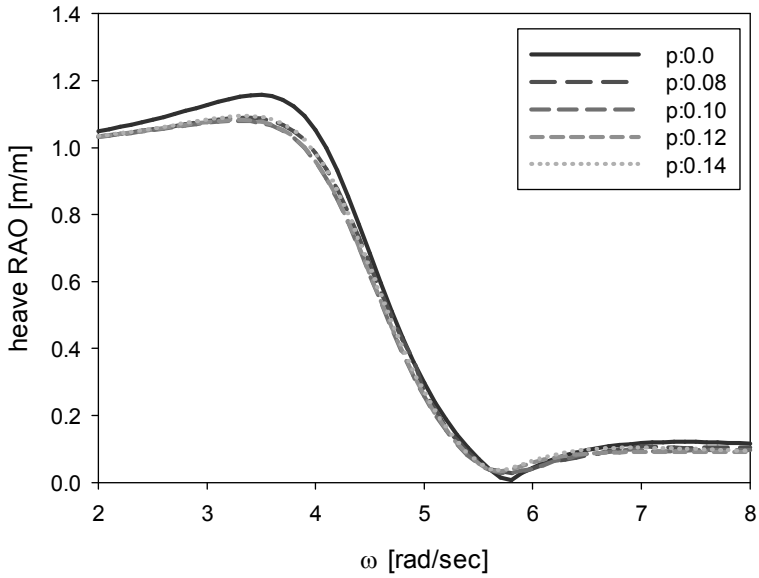

Fig.4.13. Heave RAO of the circular cylinder with dual damping plates for different porosities of the upper-damping plate at position 1 (a / b =1.6).

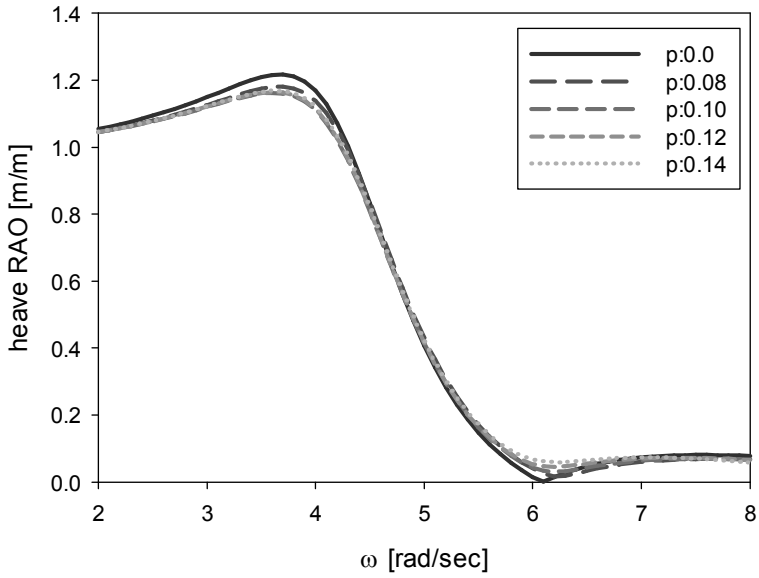

Fig.4.14. Heave RAO of the circular cylinder with dual damping plates for different porosities of the upper-damping plate at position 2 (a / b =1.6).

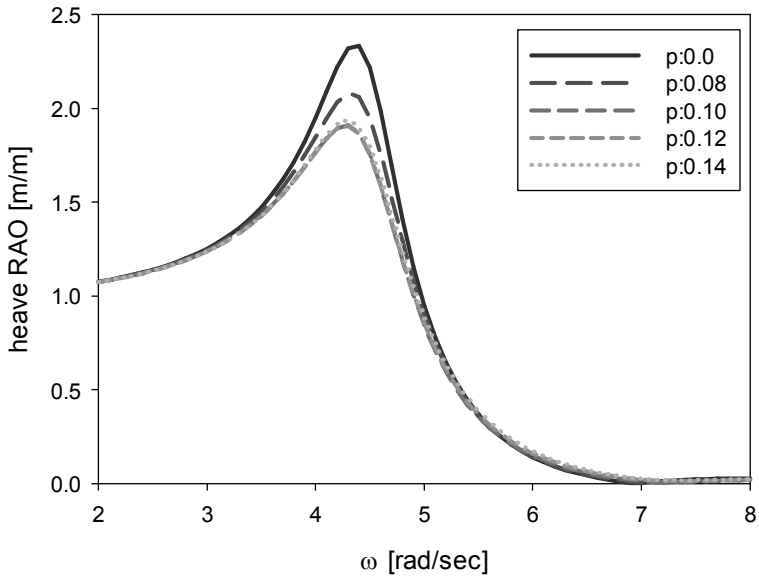

Fig.4.15. Heave RAO of the circular cylinder with dual damping plates for different porosities of the upper-damping plate at position 3 (a / b =1.6).

4.5Heave motion response in irregular waves

The experimental and analytical results of the circular cylinder without the damping plate are shown in Fig. 4. 16 (a) and (b), respectively. The solid line represents the wave signal of the 104 case (ω_p =3.0 and H_s =0.102), and the dotted one is for the time history of the heave motion of the circular cylinder. The time series of heave motion had larger values comparedto the wave signal, as it is amplified by the resonance phenomena. However, the heave motion significantly decreased when the damping plate was attachedat the bottom of the cylinder as shown in Fig. 4.17.

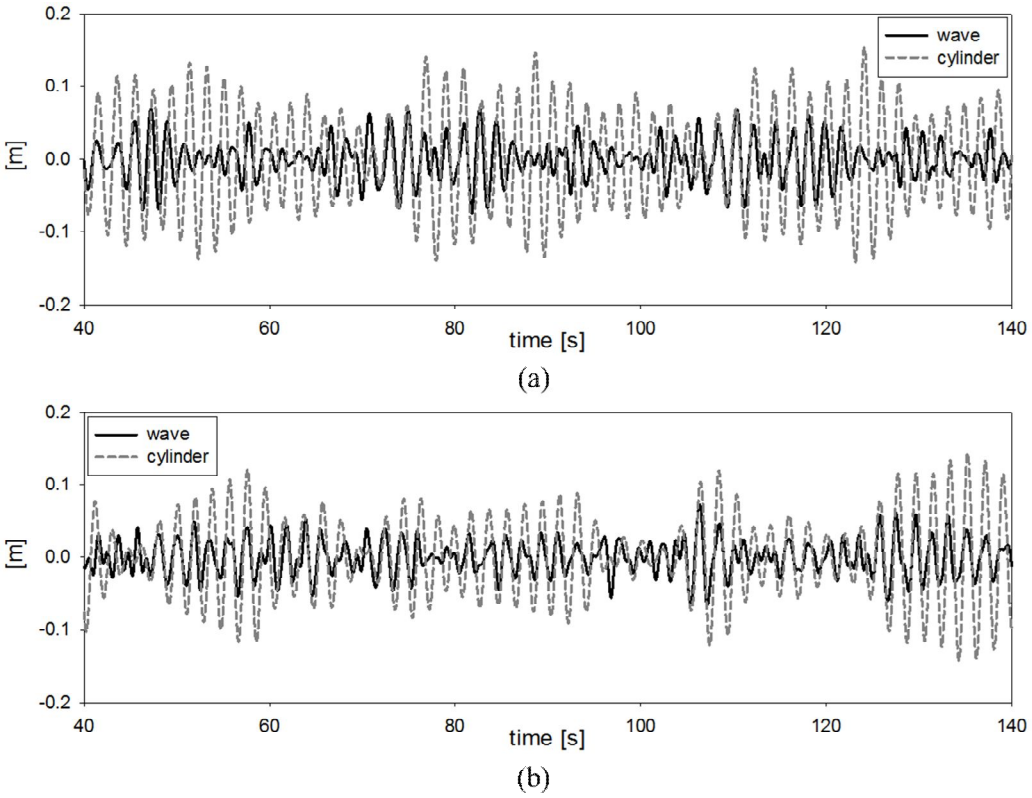

Fig.4.16. Heave motion time history of the circular cylinder without damping plate. (a) experiment, (b) MEEM. (case104: ω_p =3.0 and H_s =0.102).

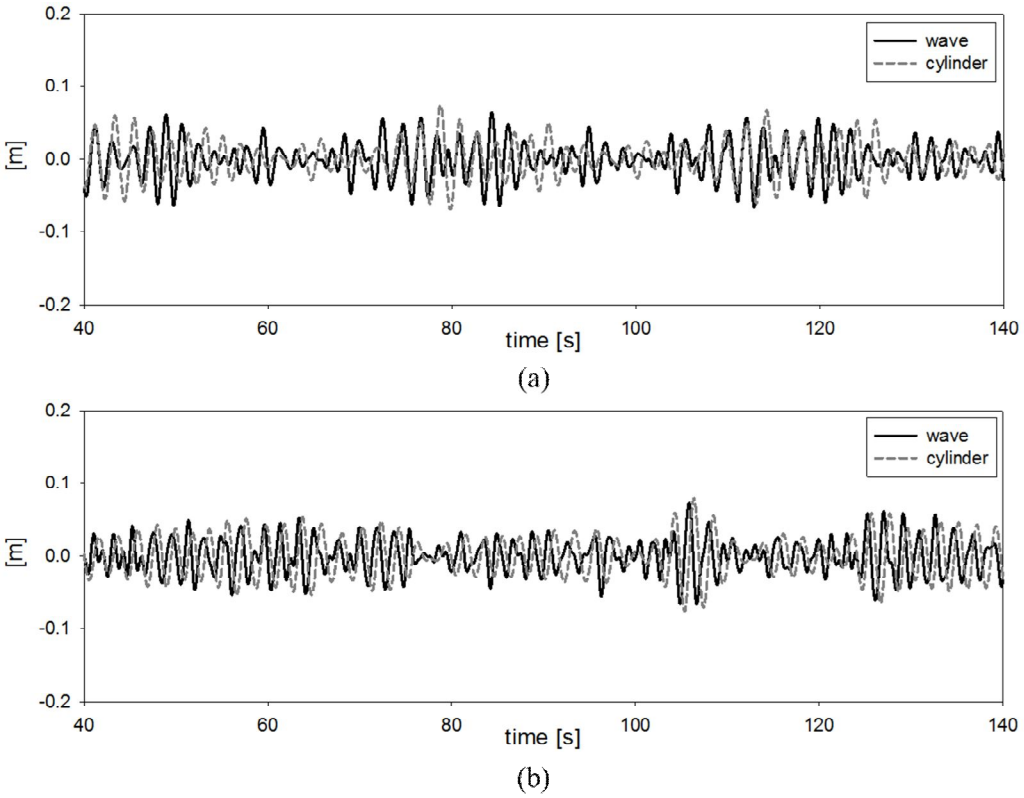

Fig.4.17. Heave motion time history of the circular cylinder with damping plate. (a) experiment, (b) MEEM. (case203: ω_p =3.0 and H_s =0.102, a/b =1.6).

Figs. 4.18 and 4.19 show the comparisons of wave and the heave motion spectrum for the circular cylinder without the damping plate and with the rigid damping plate, respectively.Red lines denote the experimental results and black ones the analytic solutions. The wave spectrum (solid line) and the heave motion spectrum (dotted line)generated by applying the FFT to the time history measuredfrom the wave height gauge and the accelerometer were in good agreement with the spectrum obtained from the analytic solution in time domain. As in the results of the regular wave experiment, the heave motion was

greatly reduced especiallyat the resonance region and the resonant frequency was shifted to the lower frequencyregion.

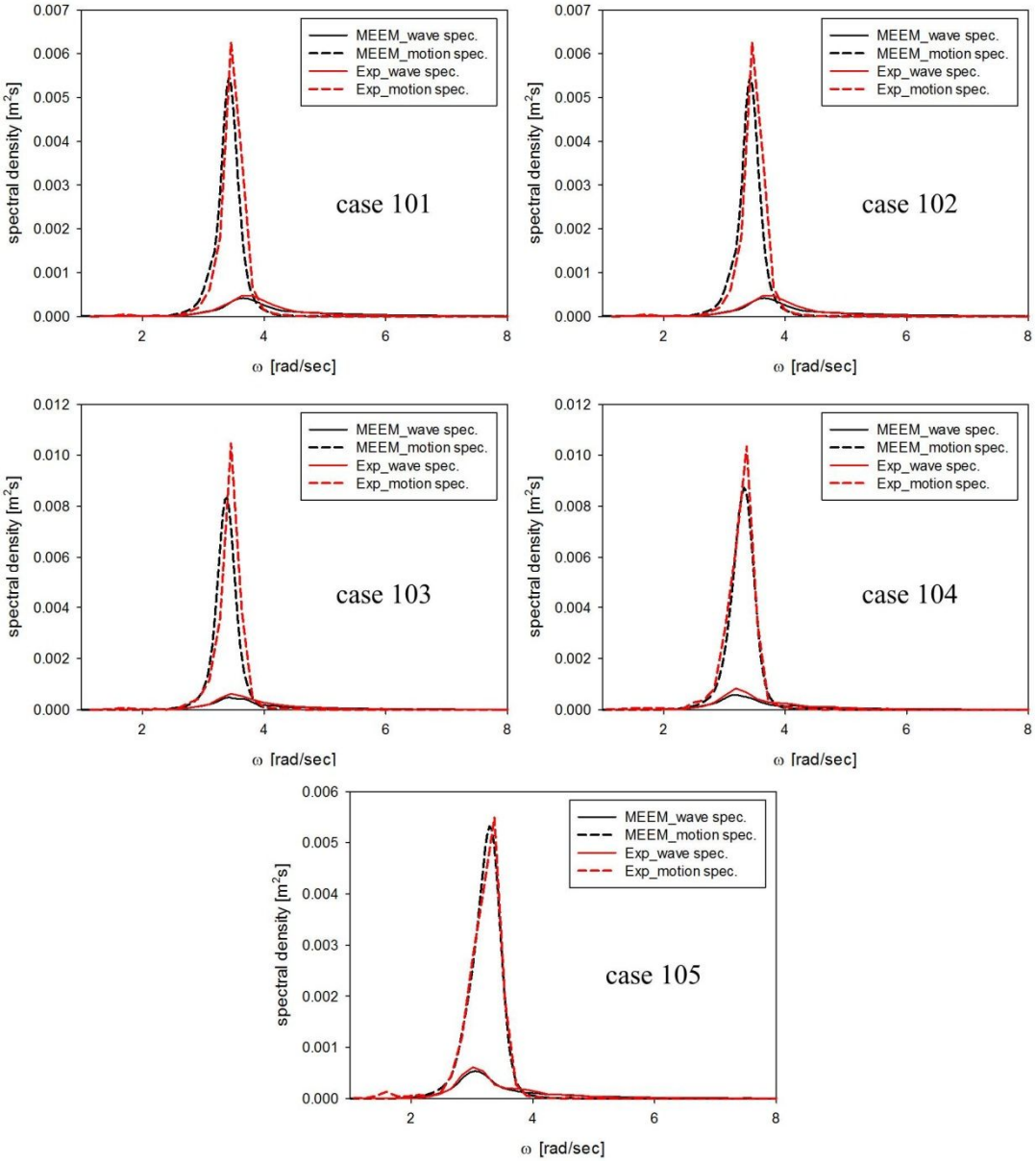

Fig.4.18.Comparison of wave and heave motion spectrum between analytic and experimental results for the circular cylinder without the damping plate.

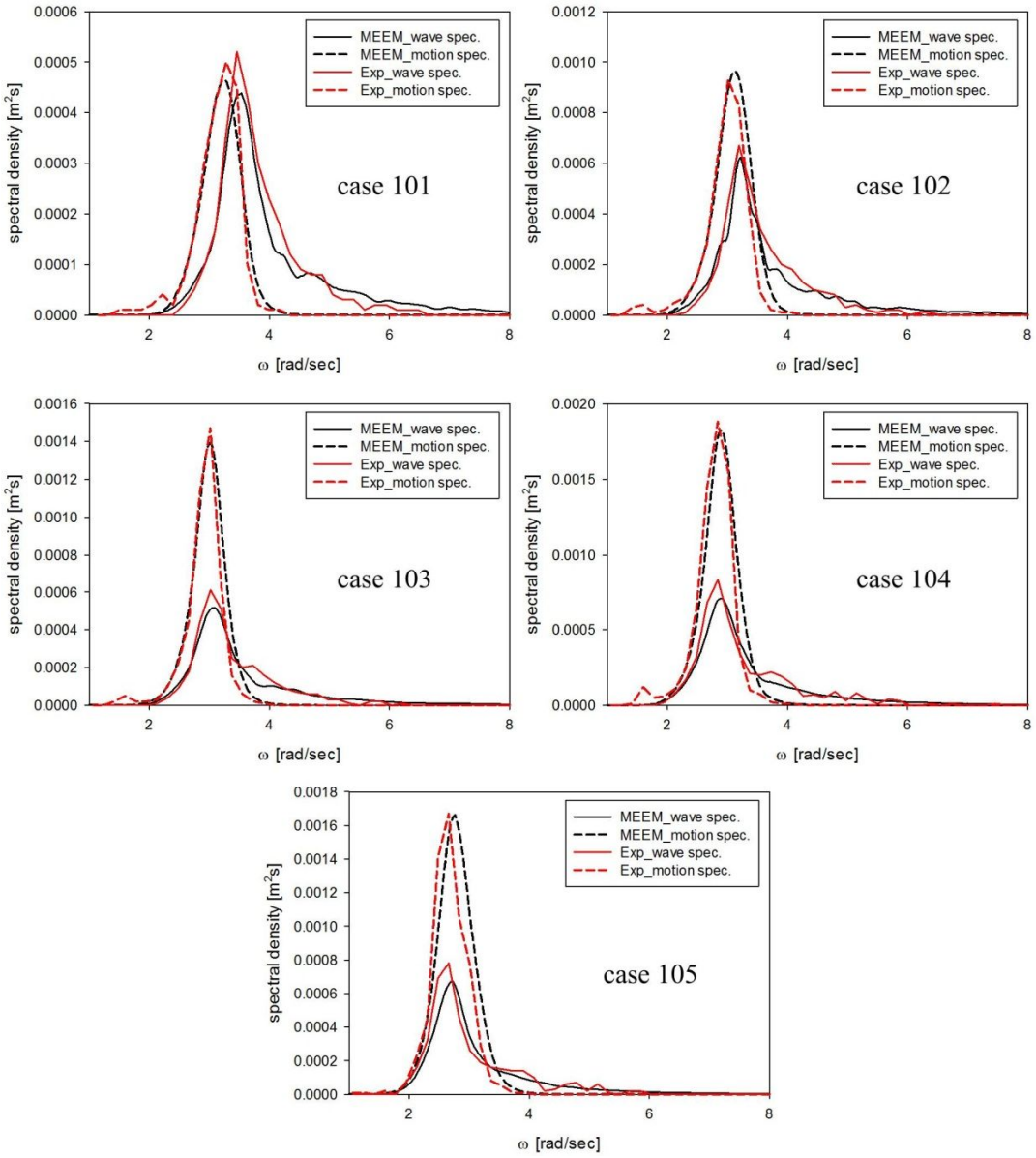

Fig.4.19.Comparison of wave and heave motion spectrum between analytic and experimental results for the circular cylinder with a rigid damping plate.

Chapter 5

APPLICATION TO A FLOATING OFFSHORE WIND TURBINE USING FAST CODE

5.1 Introduction

FAST (Fatigue, Aerodynamics, Structures, and Turbulence) is an aero-elastic simulator for horizontal-axis wind turbines used in both two- and three- bladed turbines by the National Renewable Energy Laboratory (NREL). FASTwas initially developed for the dynamic analysis of conventional land-based wind turbines. As the need for the offshore wind turbine was increased, it has been extended with additional modules for ocean environments and floating platform dynamics(Jonkman and Buhl,2005). Fig. 5.1 summarizes the modules and their interfaces.

HydroDynis a module that computes the applied hydrodynamic loads in the time domain. This module accounts for linear hydrostatic restoring; nonlinear viscous drag from incident wave kinematics, sea currents, and platform motion; the added mass and damping contributions from linear wave radiation, including free surface memory effects; and the incident wave excitation from linear diffraction in regular or irregular seas.HydroDyn was developed such that the hydrodynamic coefficients for platforms of arbitrary shape are imported from WAMIT(Wave Analysis at MIT).

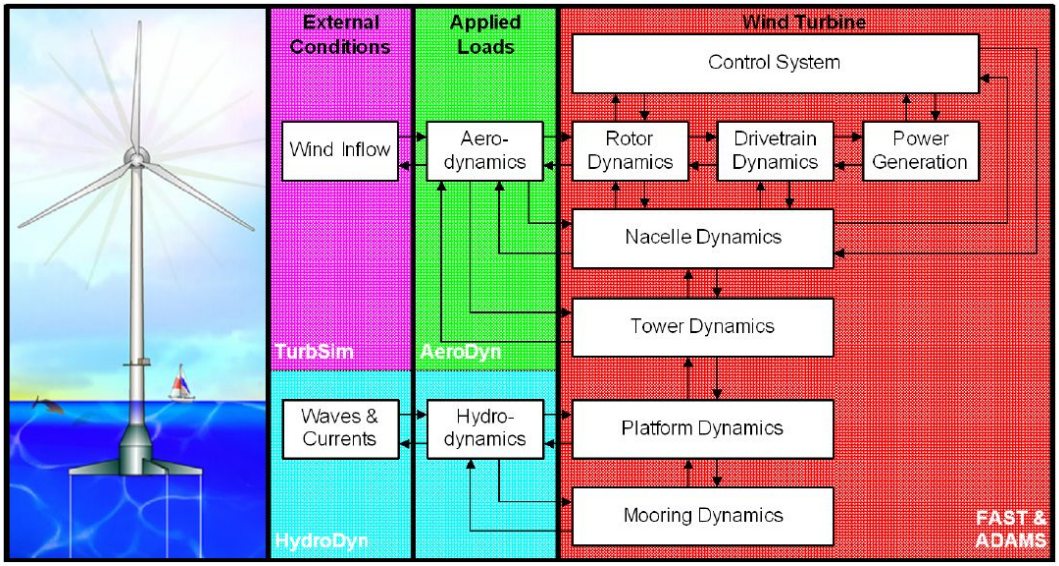

Fig.5.1. Interfacing modules to achieve aero-hydro-servo-elastic simulation (Jonkman, 2007).

5.2 Model

5.2.1Wind turbine

The wind turbine used in this study is the NREL offshore 5MW baseline wind turbine which has been adopted as the reference model for the integrated European UpWind research program. This is athree-bladed upwind horizontal-axis wind turbine. Table 5.1 summarizes the main properties of the selected wind turbine.

Table 5.1. Specifications of NREL 5MW wind turbine.

properties	unit	specification
hub height	m	90.0
tower height	m	87.6
tower diameter (top)	m	3.87
tower diameter (bottom)	m	6.5
tower mass	kg	347,460
rotor / hub diameter	m	126 / 3
cut-in / rated / cut-out wind speed	m/s	3 / 11.4 / 25
rotor mass	kg	110,000

nacelle mass	kg	220,000
blade mass	kg	17,740

5.2.2 Platform

A spar type floating support platform with single or dual damping plates, scaled up to 100 times that of the experiment model used in the free decay test of this thesis, is considered as the analysis model.To take into account the viscous effect due to the damping plate, the viscous damping calculated by the non-dimensional damping coefficient obtained fromthe heave free decay testis applied to HydroDyn. The specifications of the support platformare listed in Table 5.2.

In order to predict the heave motion response of a FOWT, it is simulated by FASTwithhydrodynamic coefficients, which were calculated by MEEM. The heave hydrodynamic coefficients and exciting forces were verified by comparison with the results of ANSYS AQWA (see Figs. 5.2–5.4). The results of the analytic solution were non-dimensionalized to adapt the output of WAMIT, the hydrodynamic pre-process program in FAST code.

The heave RAOsof the FOWT were calculated (see Fig.5.5).Along with the preceding results, the heave motion at the resonant frequency was steeply decreased by attaching the damping plate, and the resonant frequency was shifted to the low frequency region due to the

increase of the added mass.

Table 5.2. Specifications of the spar type floating platform

	FOWT only	FOWT with a single damping plate	FOWT with a rigid and porous damping plates
diameter (m)	12.00	12.00	12.00
draft (m)	26.10	26.10	26.10
mass (kg)	2,195,120	2,195,120	2,195,120
center of gravity (m)	-16.10	-16.10	-16.10
diameter ratio (a / b)	-	1.60	1.60
depth ratio (d_0 / d)	-	-	0.54
porosity of upper-plate	-	-	0.10
viscous damping (kg/s)	189,553	621,496	1,197,658

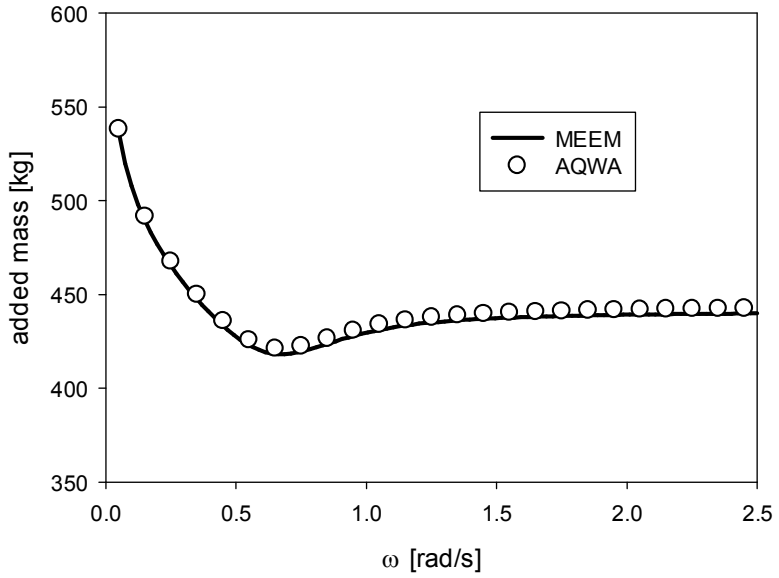

Fig.5.2. Comparison of heave added mass due to an oscillating spar type floating platform of the FOWT between analytical (MEEM) and numerical (AQWA) results.

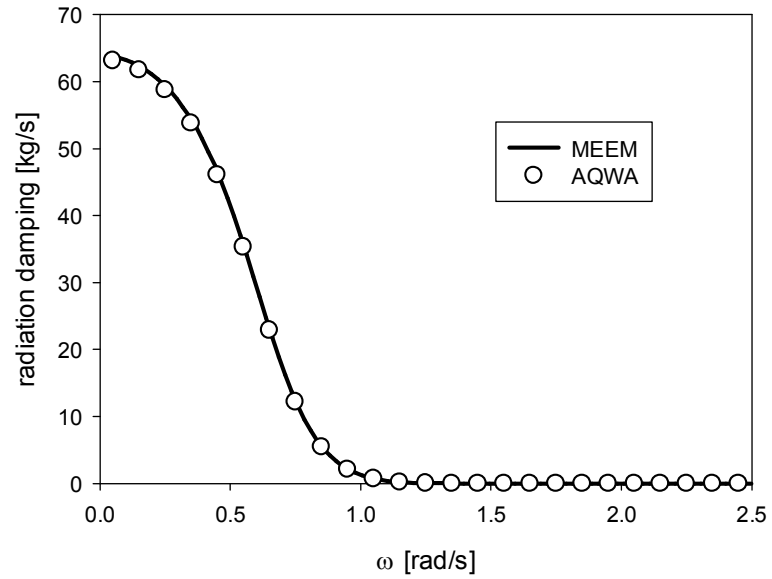

Fig.5.3.Comparison of heave radiation damping due to an oscillating spar type floating platform of the FOWT between analytical (MEEM) and numerical (AQWA) results.

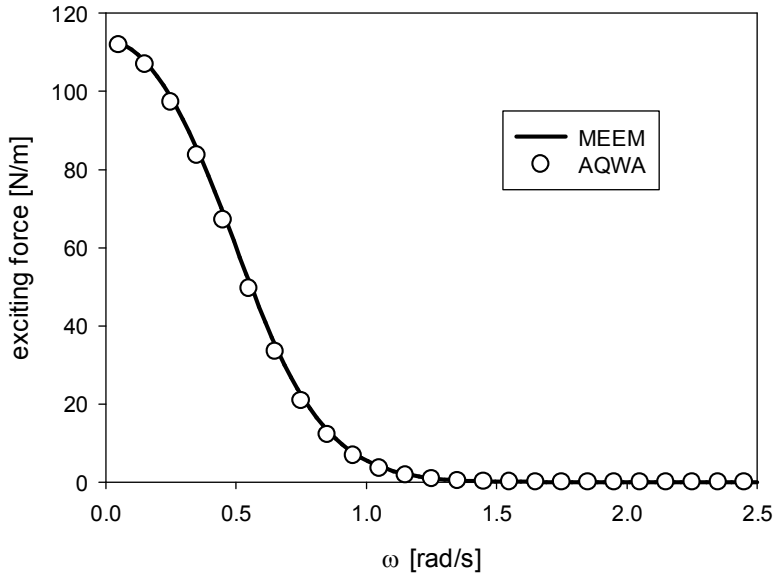

Fig.5.4.Comparison of heave wave exciting force on the spar type floating platform of the FOWT between analytical (MEEM) and numerical (AQWA) results.

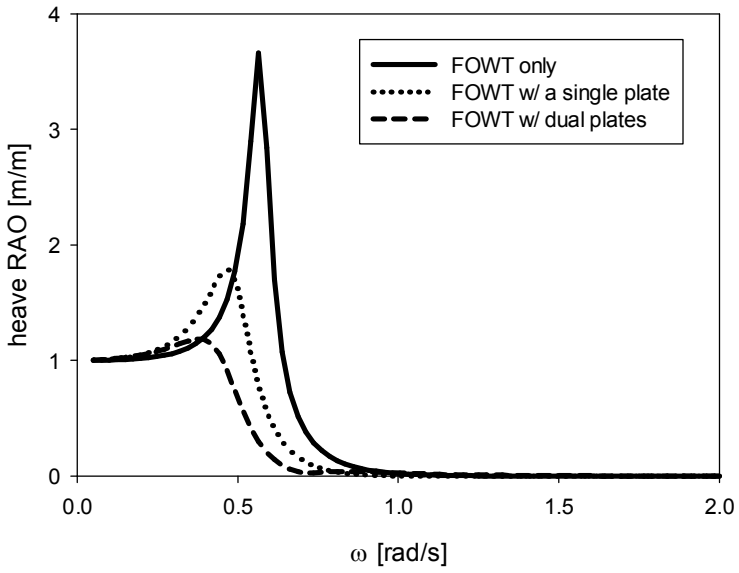

Fig.5.5. Heave RAO for the spar type FOWT with a single and dual (P = 0.1) damping plates and without a damping plate.

5.2.3 Environmental conditions

The sea states 6 and 7 applied in this research were based on the wind-wave environmental conditions listed in Table 5.3. The Normal Turbulence Model(NTM) and IEC Kaimal wind spectrum were adopted to generate the turbulent full-field three component wind condition by TurbSim v1.50 (Jonkman, 2009). The mean wind speed at 90m height was set to 11.4m/s (i.e. rated wind speed) for operating condition and 25.0m/s (i.e. cut-out wind speed) for parked condition. The turbulence intensity (I_{ref}) was set to 14%.The JONSWAP spectrum ($\gamma = 3.3$) was used to generate the irregular waves(see Fig. 5.6),and the water depth was assumed to be constant at 200m(see Figs. 5.7 and 5.8).

Table 5.3. Environmental conditions for each sea state.

turbine condition	sea state	V_{mean} (m/s)	H_s (m)	T_p (s) (ω_p (rad/s))
power production	6	11.4	5.00	12.4 (0.507)
	7		7.50	15.0 (0.419)
parked	7	25.0	7.50	15.0 (0.419)

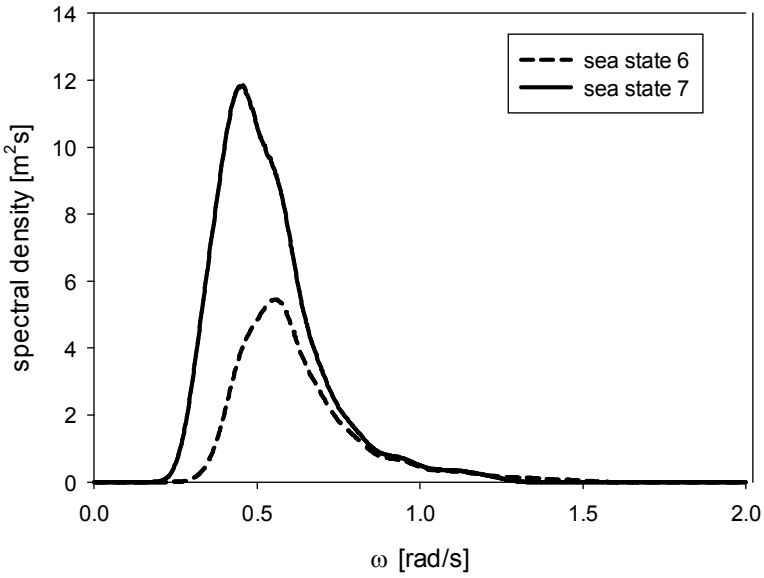

Fig.5.6.JONSWAP wave spectrum ($\gamma = 3.3$) for each sea state.

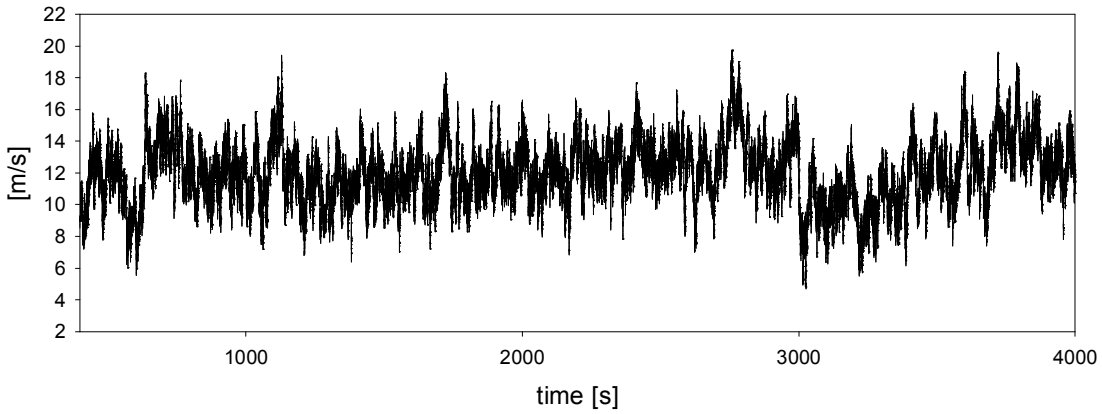

Fig.5.7. Wind speed time history ($V_{mean} = 11.4\frac{m}{s}$, $I_{ref} = 0.14$).

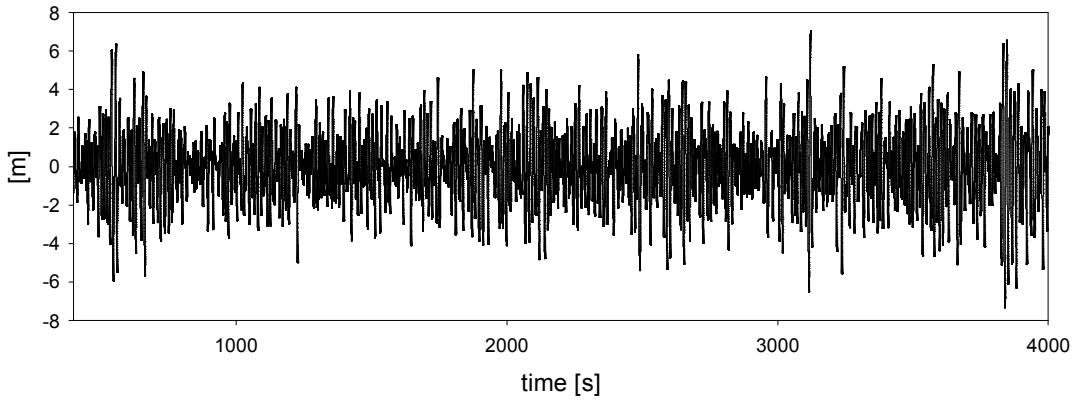

Fig.5.8. Wave elevation time history ($H_s = 7.50\frac{m}{s}$, $T_p = 15.0\,\mathrm{sec}$).

5.3 Results

In this study, the analysis was for the FOWT calculation model without the mooring, and only heave motion was taken into account. The other parts of the wind turbine system were set to operate normally.

Fig. 5.9 presents the calculation results of the heave motion time history in sea state 6. Fig. 5.9 (a) is the case of the FOWT without the damping plate, (b) is the one with a single damping plate at the bottom, and (c) is the result of the FOWT with the rigid and porous damping plates. As the figures show, the heave motion of the FOWT was considerably decreased because of the damping plate, and, especially, the smallest heave motion occurred in the case of the dual damping plates. Fig. 5.10 shows the calculation results for sea state 7, and the results were concurrent with those of sea state 6. The spectral results obtained from the FFT of the time history resultsin sea states 6 and 7 are shown in Figs. 5.11 and 5.12, respectively. The significant reduction of the heave energy of the FOWT is presented in these results.

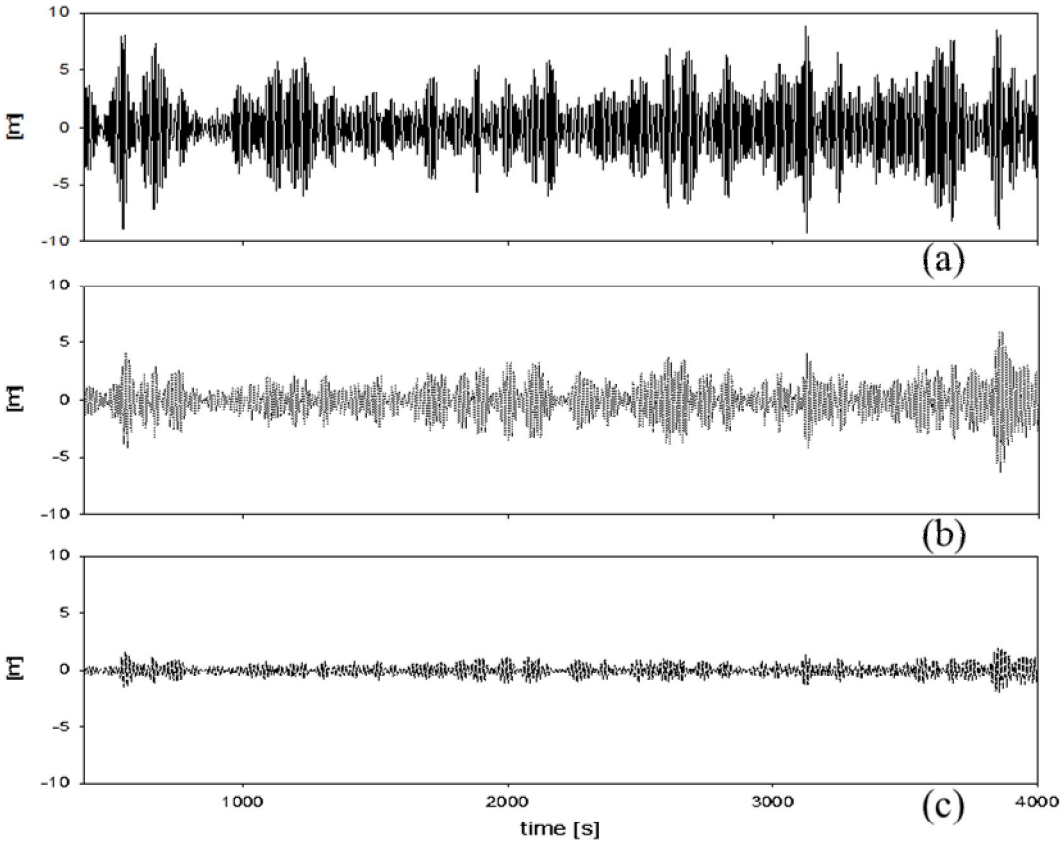

Fig.5.9. Heave motion time history of the FOWT for sea state 6 (H_s =5.0 m, T_p =12.4 sec). (a) without a damping plate, (b) with a single rigid damping plate (a/b =1.6), (c) with dual (rigid + porous) damping plates (a/b =1.6, d_0/d =0.54, P =0.1).

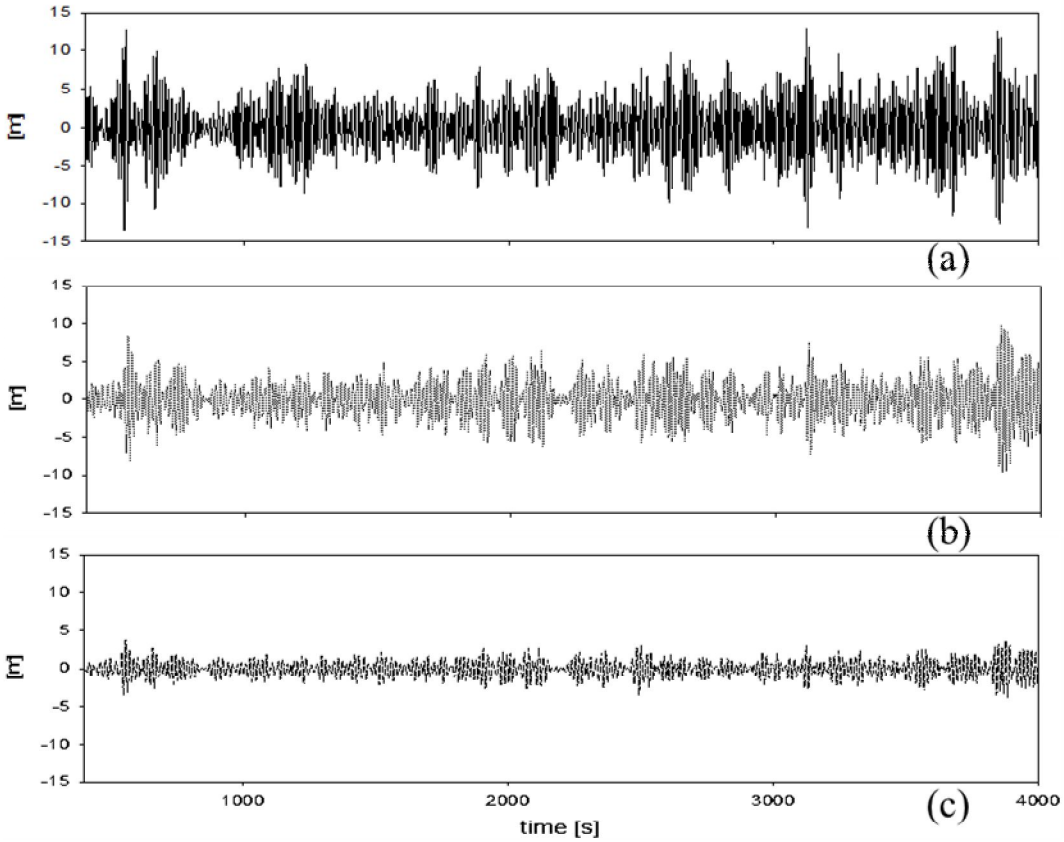

Fig.5.10. Heave motion time history of the FOWT for sea state 7 (H_s =7.5 m, T_p =15.0 sec). (a) without a damping plate, (b) with a single rigid damping plate (a/b =1.6), (c) with dual (rigid + porous) damping plates (a/b =1.6, d_0/d =0.54, P =0.1).

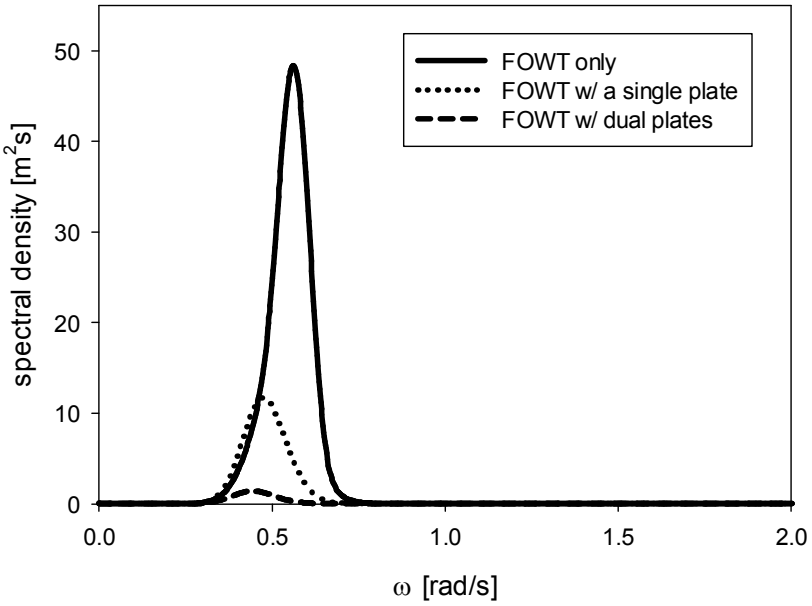

Fig.5.11. Heave motion spectrum of the spar type FOWT with a single and dual (d_0 / d =0.54, P =0.1) damping plates and without a damping plate (a / b =1.6) for sea state 6 (H_s =5.0 m, T_p =12.4 sec).

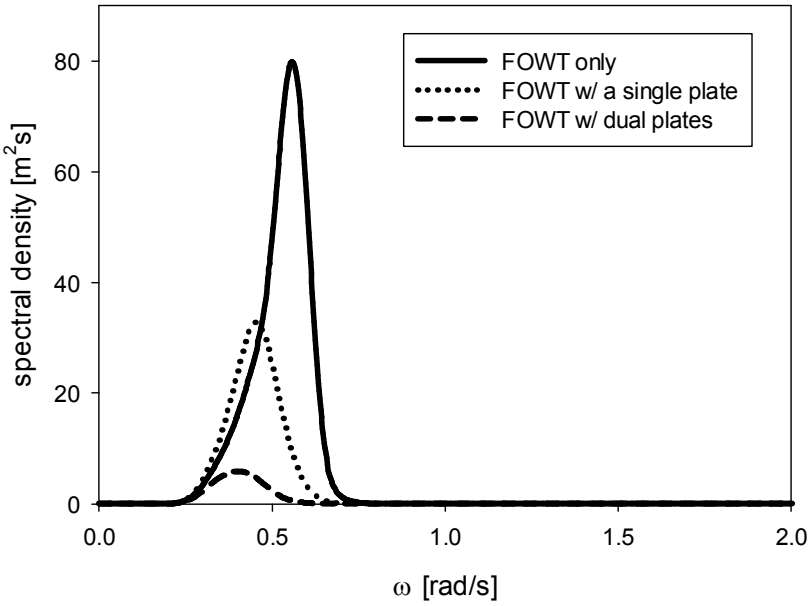

Fig.5.12. Heave motion spectrum of the spar type FOWT with a single and dual (d_0 / d =0.54, P =0.1) damping plates (a / b =1.6) and without a damping plate for sea state 7 (H_s =7.5 m, T_p =15.0 sec).

To examine statistically the heave motion reduction characteristics of the FOWT depending on the existence of the damping plate, the significant heave motion height was calculated (see Table 5.4). The significant heave motion height is the result obtained from the statistics process of the calculation results of the time history by zero-crossing method. Compared to the FOWT without the damping plate, the single damping plate caused an average decrease in the heave motion to 38%, and 76% with the dual plates during the power production process.In addition, it is similar to the parked condition of the wind turbine and the operating condition at sea state 7.

Table 5.4. Statistical analysis results of the wave and the heave motion of the FOWT.

turbine condition	sea state	model	significant wave height (m)	significant heave motion height (m)	significant heave response amplitude
power production	6	FOWT	5.004	9.957	1.990
		FOWT w/ a single plate		5.349	1.069
		FOWT w/dual plates		1.895	0.379
	7	FOWT	7.374	13.770	1.867
		FOWT w/ a single plate		9.564	1.297
		FOWT w/dual plates		4.137	0.561
parked	7	FOWT	7.374	13.843	1.877
		FOWT w/ a single plate		9.586	1.300
		FOWT w/dual plates		4.152	0.563

Due to the decrease of the heave motion, the variation of the axial force at the tower base, yaw bearing, and blade root also significantly decreased (Figs. 5.13–5.15). The standard deviations of the axial force on the locations of the FOWT with the dual damping plates decreased more than 81% compared to the case of the FOWT alone (see Table 5.5). This can be an advantage to extend the fatigue life of the whole wind turbine system as well aseach part, while there was no differencein the generated power between the models,since only heave motion of the FOWT was considered (see Fig. 5.16).

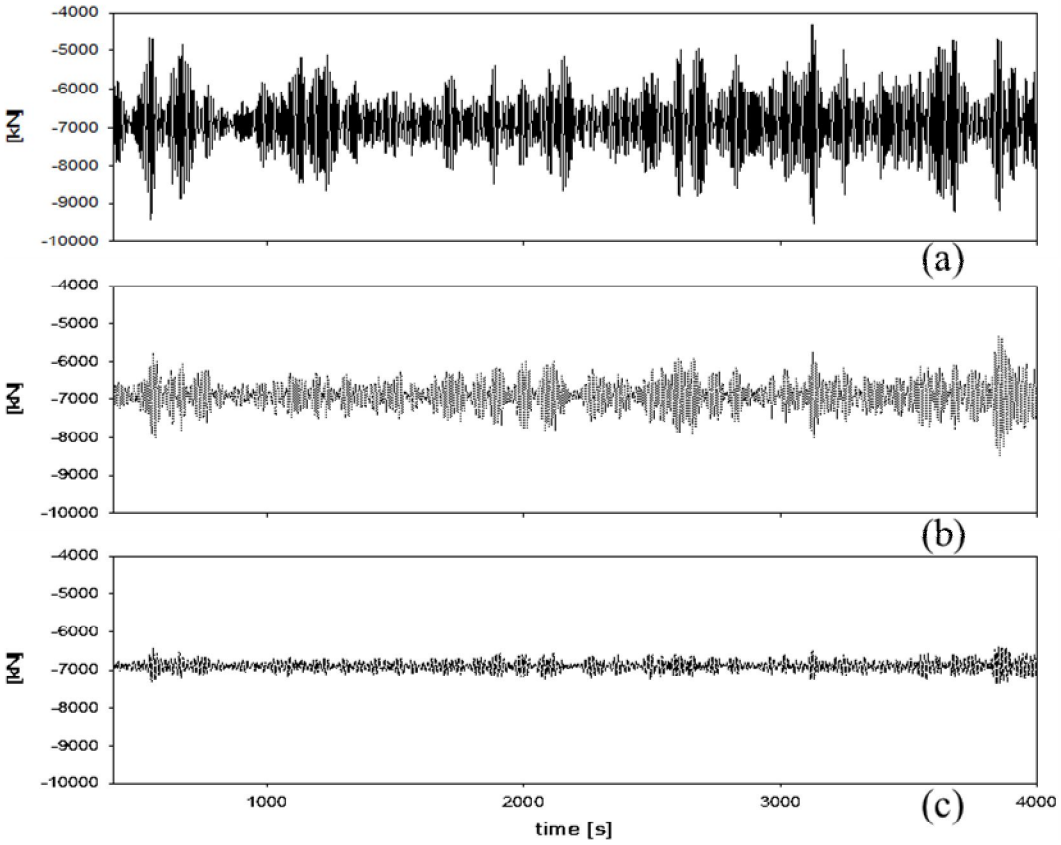

Fig.5.13. The tower base axial force time history of the FOWT for sea state 7 (H_s=7.5 m, T_p=15.0 sec). (a) without a damping plate, (b) with a single rigid damping plate (a/b=1.6), (c) with dual (rigid + porous) damping plates (a/b=1.6, d_0/d=0.54, P=0.1).

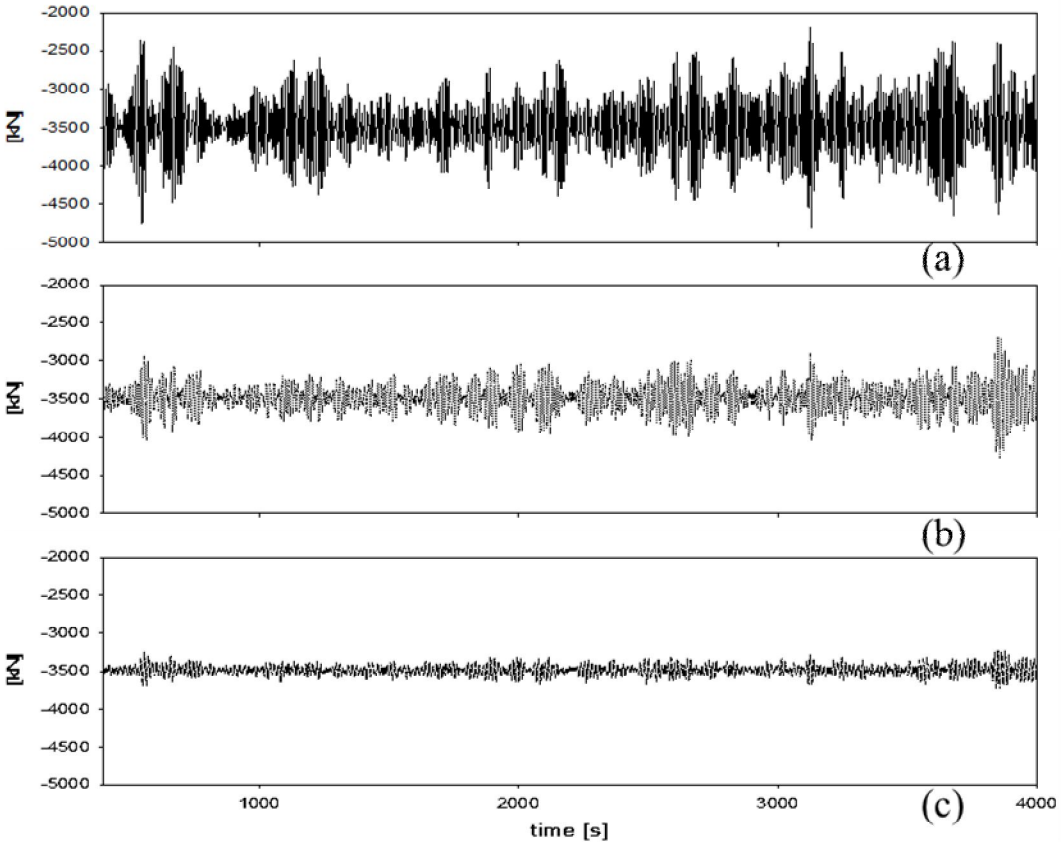

Fig.5.14. The yaw bearing axial force time history of the FOWT for sea state 7 (H_s =7.5 m, T_p =15.0 sec). (a) without a damping plate, (b) with a single rigid damping plate (a/b =1.6), (c) with dual (rigid + porous) damping plates (a/b =1.6, d_0/d =0.54, P =0.1).

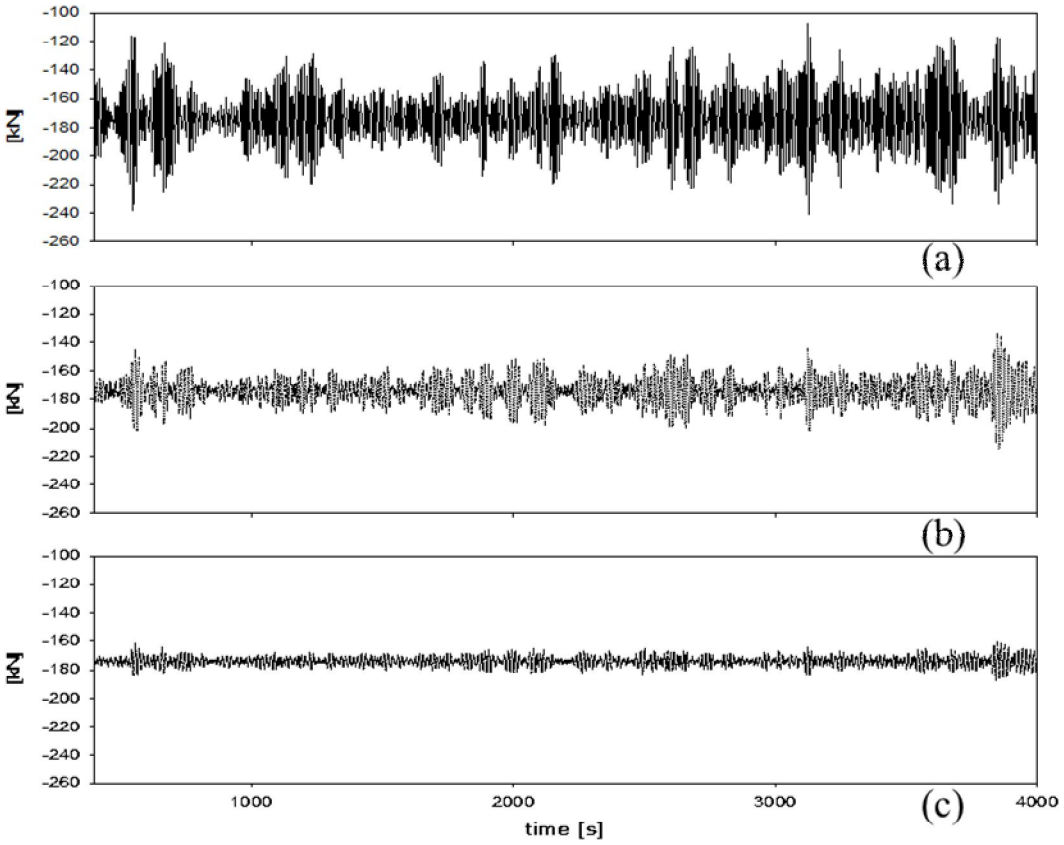

Fig.5.15. The blade root axial force time history of the FOWT for sea state 7 (H_s=7.5 m, T_p=15.0 sec) in parked condition. (a) without a damping plate, (b) with a single rigid damping plate (a/b=1.6), (c) with dual (rigid + porous) damping plates (a/b=1.6, d_0/d=0.54, P=0.1).

Table 5.5. Statistical analysis results of the axial forces on the FOWT.

position	model	mean (kN)	max (kN)	min (kN)	σ_f (kN)
tower base	FOWT	-6897.02	-9526.00	-4303.00	696.13
	FOWT w/ a single plate	-6897.60	-8475.00	-5323.00	352.36
	FOWT w/dual plates	-6897.30	-7385.00	-6386.00	128.44
yaw bearing	FOWT	-3485.45	-4806.00	-2178.00	349.31
	FOWT w/ a single plate	-3485.73	-4282.00	-2695.00	177.12
	FOWT w/dual plates	-3485.57	-3731.00	-3229.00	65.66
blade root	FOWT	-174.02	-241.30	-107.70	17.81
	FOWT w/ a single plate	-174.03	-214.90	-133.60	8.98
	FOWT w/dual plates	-174.02	-187.40	-160.70	3.27

σ_f : standard deviation

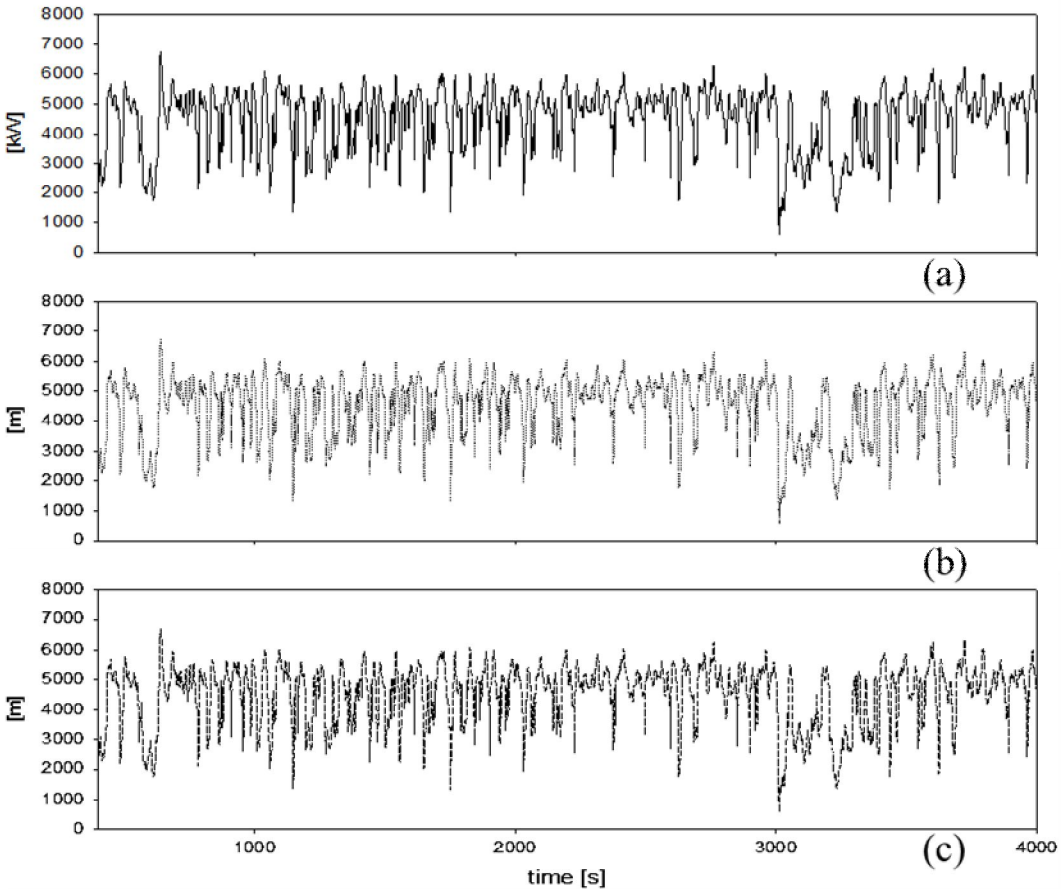

Fig.5.16. The generated power time history of the FOWT for sea state 7 (H_s=7.5 m, T_p=15.0 sec). (a) without a damping plate, (b) with a single rigid damping plate (a/b=1.6), (c) with dual (rigid + porous) damping plates (a/b=1.6, d_0/d=0.54, P=0.1).

Chapter 6

CONCLUSIONS AND FUTURE WORK

In this research,the heave motion response of a floating circular cylinderwith a damping plate as a motion reduction appendage is investigated both analytically and experimentally.In order to analyze the heave motion characteristics of the circular cylinder with combination of a single and dual damping plates or rigid and porous damping plate, ananalytic method using Matched Eigenfunction Expansion Method (MEEM)was employed.In case of the porous damping plate, the energy dissipation effect is modeled by Darcy's law. The analytic solutions by MEEM are compared against a series of laboratory experiments performed in a 2-D wave flume for regular waves, and alarge scaled wave flume for irregular waves. Overall, the agreement between the analytic and experiment is good. This supportsthe strong confirmation that the analytic method derived in this thesis is reasonableto verify the effect of the damping plate to the heave motion of a cylinder body.

The importantconclusions concerning the damping plate effectinclude that the significant increases in the viscous and radiation damping by attaching the damping plate leadto the considerable reduction of heave motion amplitude near the resonant frequency region and the shift of the resonant frequency to the low frequency region due to the increase in the added mass. More specifically, with the diameter ratio (the ratio between the damping plate and cylinder diameter) less than 1.6 and the depth ratio (the submerged depth ratio

between the upper and lower damping plate) less than the specific value, the viscous damping tends to increase considerably, while the effect of the porosity is insignificant because theheave motion of the cylinder is overdampedby the dual damping plate,ifspacing apart is larger than the critical distance.

In the applicationof the FOWT, the analytic solutions of the added mass, radiation damping, and wave exciting force of the floating support structure of the FOWT by MEEM are observed to be in a good agreement with the numerical calculation results from ANSYS AQWA. In this study,the results of the analytic solution are non-dimensionalized to form the WAMIT output as the hydrodynamic input data (added mass, radiation damping, and wave exciting force) to HydroDyn, hydrodynamics module of FAST code. The simulation result for the heave motion in the case of the FOWT with dual damping plates is drastically decreased than the FOWT only. Thisleadsto the large decrease in the variation of axial force at the parts of the FOWT. This can be an advantage to extend the fatigue life of the whole wind turbine system as well as each part, while the decrease in the heave motion hardly affects the power generation.

In order to analyze the realistic motion characteristics and powerperformance of the FOWT, amotion analysis program will be developed considering 6 DOF motions and the mooring line dynamics based on the results of this thesis.

REFERENCES

Bai, K.J., 1977. The added mass of two-dimensional cylinders heaving in water of finite depth.Journal of Fluid Mechanics. 81, 85–105.

Cho, I.H., 2011. Hydrodynamic forces characteristics of a circular cylinder with a damping plate. J. Ocean Engineering and Technology. 25(1), 1–7.

Cho, I.H., Kim, M.H., 2008. Wave absorbing system using inclined perforated plates. Journal of Fluid Mechanics. 608, 1–20.

Chwang, A.T., 1983. A porous wavemaker theory.Journal of Fluid Mechanics. 132, 395–406.

Chwang, A.T., Wu, J., 1994. Wave scattering by submerged porous disk. Journal of Engineering Mechanics. 120, 2575–2587.

Cummins, W.E., 1962. Impulse response function and ship motions. Schiffstechnik 9 (1661), 101–109

Downie, M., Graham, J., Hall, C., Incecik, A.,Nygaard, I., 2000 Anexperimental investigation of motion control devices for trussspars. Marine Structures. 13,75–90.

Garrett, C.J.R., 1971. Wave forces on a circular dock. Journal of Fluid Mechanics. 46, 129–139.

Havelock, T.H., 1955. Waves due to a floating sphere making periodic heaving oscillations.Proceedings of the Royal Society of London. 231, 1–7.

Heronemus, W. E., 1972. Pollution-Free Energy From Offshore Winds.8th Annual Conference and Exposition Marine Technology Society. Washington D.C., USA.

Jonkman, B.J., 2009. TurbSim user's guide: Version 1.50. National Renewable Energy Laboratory.Golden, CO.

Jonkman, J.M., 2007. Dynamic modeling and loads analysis of an offshore floating wind turbine. Ph.D. Thesis, Department of Aerospace Engineering Sciences, University of Colorado, Boulder, CO.; National Renewable Energy Laboratory. Golden, CO.

Jonkman, J.M., Buhl Jr., M.L., 2005. FAST User's guide.National Renewable Energy Laboratory.Golden, CO.

Jonkman, J., Butterfield, S., Musial, W., Scott, G., 2009. Definition of a 5-MW reference wind turbine for offshore system development.National Renewable Energy Laboratory.Golden, CO.

Journée, J.M.J., Massie, W.W., 2001. Offshore Hydromechanics. Lecture notes, Delft University of Technology, Netherlands.

Koh, H.J., Cho, I.H. 2011.Motion response of a circular cylinder with a heave plate in waves. In: Proceedings of the 21st International Offshore and Polar Engineering Conference. Maui, Hawaii.

Kritis Ir. B., 1979. Heaving motion of axisymmetric bodies.Journal of Ship Research. 5, 26–27

Larsen, T.J., Hanson, T.D., 2007. A method to avoid negative damped low frequent tower vibrations for a floating, pitch controlled wind turbine. Journal of Physics: Conference Series, The Second Conference on The Science of Making Torque From Wind. Copenhagen, Denmark.

Magee, A., Sablok, A., Maher, J., Halkyard, J., Finn, L., Datta, I., 2000. Heave plate effectiveness in the performance of truss spars. In: Proceedings of the ETCE/OMAE 2000 Joint Conference. New Orleans, LA, USA.

McIver, P., Evans, D.V., 1984. The occurrence of negative added mass in free-surface problems involving submerged oscillating bodies.Journal of Engineering Mechanics. 18, 7–22.

Mei, C.C., Black, J.L., 1969. Scattering of surface waves by rectangular obstacles in waters of finite depth.Journal of Fluid Mechanics. 38, 499–511.

Mei, C.C., Liu, P.L.F., Ippen, A.T., 1974. Quadratic loss and scattering of long waves.Journal of the Waterways, Harbors, and Coastal Engineering Division. 100, 217–239.

Molin, B., Nielsen, F.G., 2004. Heave added mass and damping of a perforated disk below the free surface. Proc. 19th Int. Workshop on Water Waves and Floating Bodies.Cortona, Italy.

Myhr A., Maus K.J., Nygaard T.A.,2011. Experimental and computational comparisons of the OC3-hywind and tension-leg-buoy (TLB) floating wind turbine conceptual designs. In: Proceedings of the 21stInternational Offshore and Polar Engineering Conference. Maui, Hawaii.

Nielsen, F.G., Hanson, T.D., Skaare, B., 2006. Integrated dynamic analysis of floating offshore wind turbines.In: Proceedings of 25th International Conference on Offshore Mechanics and Arctic Engineering. Hamburg, Germany.

Rho, J.B., Choi, H.S., 2002. Heave and pitch motions of a spar platform with damping plate. In: Proc. 12thProceedings of the International Offshore and Polar Engineering Conference. Kitakyushu, Japan, 198–201.

Sadeghi, K., Incecik, A., Downie, M.J., 2004. Response analysis of a truss spar in the frequency domain. Marine Science and Technology. 8, 126–137.

Skaare, B., Hanson, T.D., Nielsen, F.G., 2007. Importance of control strategies on fatigue life of floating wind turbines. In: Proceedings of 26th International Conference on Offshore Mechanics and Arctic Engineering. San Diego, CA.

Shin, H., 2011.Model test of the OC3-hywind floating offshore wind turbine.In: Proceedings of the 21stInternational Offshore and Polar Engineering Conference. Maui, Hawaii.

Stansberg, C.T., Nygaard, I., Ormberg, H., Downie, M.J., 2001. Deep-water truss spar in waves and current-experiment vs. time-domain coupled analysis.Deep Offshore Technology Conference. Rio de Janeiro, France.

Sudhakar, S., Nallayarasu, S., 2013.Hydrodynamic response of spar with single and double heave plates in regular waves.International Journal of Ocean System Engineering. 3(4), 188–208.

Sudhakar, S., Nallayarasu, S., 2014. Hydrodynamic responses of spar hull with single and double heave plates in random waves. International Journal of Ocean System Engineering. 4(1), 1–18.

Tao, L.,Cai, S., 2004. Heave motion suppression of a spar with a heave plate. Ocean Engineering. 31(5–6), 669–692.

Tao, L., Dray, D., 2008. Hydrodynamic performance of solid and porous heave plates.Ocean Engineering. 35(10), 1006–1014.

Tao, L., Molin, B., Scolan, Y.M.,Thiagarajan, K.2007. Spacing effects on hydrodynamics of heave plates onoffshore structures.Journal of Fluids andStructures.23(8), 1119–1136.

Thiagarajan, K.P.,Troesch, A.W., 1998. Effects of appendages and small currents on the hydrodynamic heave damping of TLP columns. Journal of Offshore Mechanics and Arctic Engineering. 120(1), 37–42.

Tuck, E.O., 1975. Matching problems involving flow through small holes. Advances in Applied Mechanics. 15, 89–158.

Tung, C.C., 1979. Hydrodynamic forces on submerged vertical circular cylindrical tanks under ground excitation. Applied Ocean Research. 1, 75–78.

Wang, K.H., Ren, X., 1994. Wave interaction with a concentric porous cylinder system.Ocean Engineering. 21(4), 343–360.

Waris, M.B., Ishihara, T., 2012.Dynamic response analysis of floating offshore wind turbine with different types of heave plates and mooring systems by using a fully nonlinear model.Coupled Systems Mechanics. 1(3), 247–268.

Yeung, R.W., 1975. A hybrid integral-equation method for time harmonic free surface flow.1st Int. Conf. Numer.Ship Hydrodynamics. Gaithersburg, Maryland.

Yeung, R.W., 1981. Added mass and damping of a vertical cylinder in finite-depth waters.Applied Ocean Research. 3(3), 119–133.

Yu, X., 1995. Diffraction of water waves by porous breakwaters. Journal of Waterway,Port,Coastal, and Ocean Engineering. 121(6), 275–282.

ACKNOWLEDGEMENT (IN KOREAN)

그동안의대학원생활을되돌아보며짧지않은기간동안참많은분들께서큰도움을주어논문이완성될수 있었기에이기회를빌어감사의말을전합니다.

우선부족한저를여기까지이끌어주시고모든일의모범이되어주신조일형교수님께깊은감사를드립니다. 교수님께서저에게베풀어주신은혜를다갚을수없겠지만, 항상보답하는마음으로최선을다하는삶을살도록노력하겠습니다.

그리고심사위원장을맡아주시고풍력대학원의발전을위해서끊임없이노력하시는허종철교수님께도진심 으로감사드립니다.

바쁘신와중에심사를맡아주신한국에너지기술연구원의경남호박사님께다시한번감사드립니다.

모든학생들에게언제나노력하는자세를보여주시는팽동국교수님과짧은시간이지만논문을위해많은조언 을해주신배윤혁교수님께도심사를맡아주심에대해감사의말씀을드립니다.

또한대학원생활을하는동안많은가르침과조언을주신이종현교수님, 배진호교수님, 김준영교수님,유원선교수님과경주대학교권혁민교수님께도진심으로감사를드립니다.

선배의뒤를받쳐주느라고생했던해양공학실험실후배정록이, 혜빈이, 종우너희들덕분에긴시간의마침을찍는다. 해양시스템공학과의믿음직한대학원생주호와재일이, 정신적지주이신남권호박사님과행복한쌍둥이아빠태훈이,한국해양대에서무사히박사과정마치길바라는 승우,토목공학과승현이, 건설기술연구원의박민수박사님, 풍력대학원상현형님과정우를비롯한모든동기및후배여러분들에게도감사의말을전합니다.

그리고지치고힘들때응원해준나의친구들승종, 윤승, 경원, 정운, 승환, 성헌아고맙다.

언제나저를믿어주시고기도해주시는아버지와어머니께사랑의마음을드리며, 오래도록건강하게저희곁에계셔주시길간절히기도드립니다.

그리고묵묵히믿음으로응원해주신장모님께도깊은감사를드립니다. 형님과형수님, 하나뿐인조카현민이, 그리고동생범준에게도이자리를빌어사랑의마음을전합니다.

끝으로사랑하는나의아내성화와나의아들현우에게이논문을바칩니다.